Summer 1-1-2020

Defect And Disorder In Dendritic Arrays Solidified on Earth And on the Space Station

Shirin Khan
Cleveland State University

Recommended Citation

Khan, Shirin, "Defect And Disorder In Dendritic Arrays Solidified on Earth And on the Space Station" (2020). *ETD Archive*. 1265.
https://engagedscholarship.csuohio.edu/etdarchive/1265

DEFECT AND DISORDER IN DENDRITIC ARRAYS SOLIDIFIED ON EARTH AND ON THE SPACE STATION

SHIRIN KHAN

Bachelor of Technology in Chemical Engineering

Laxminarayan Institute of Technology

May 2017

Submitted in partial fulfillment of requirements for the degree

MASTER OF SCIENCE IN CHEMICAL ENGINEERING

at the

CLEVELAND STATE UNIVERSITY

August 2020

We hereby approve this thesis

for

SHIRIN KHAN

Candidate for the Master of Science in Chemical Engineering degree for the

Department of Chemical and Biomedical Engineering

and

CLEVELAND STATE UNIVERSITY's

College of Graduate Studies by

____

Surendra Tewari, Ph.D., Dissertation Chairperson

Department of Chemical & Biomedical Engineering, June 9, 2020

Department & Date

____

Jorge E. Gatica, Ph.D.,Dissertation Committee Member

Department of Chemical & Biomedical Engineering, June 9, 2020

Department & Date

____

Miron Kaufman, Ph.D., Dissertation Committee Member

Department of Physics, June 9, 2020

Department & Date

July 9, 2020
Student's Date of Defense

ACKNOWLEDGMENTS

First and foremost, I would like to express my deep and sincere gratitude to my thesis advisor Prof. Surendra Tewari for giving me the opportunity to do research and providing invaluable guidance throughout my master's research. His dynamism, vision, sincerity, and motivation have deeply inspired me. He has taught me the methodology to carry out the research and to present the research works as clearly as possible. It was a great privilege and honor to work and study under his guidance. Besides my advisor, I would like to thank the rest of my thesis committee: Prof. Jorge E Gatica and Prof. Miron Kaufman, for taking out time to read my thesis and for being supportive. My sincere thanks also go to all Professors from the Chemical and Biomedical Engineering Department as I have tried applying whatever I learned through them by means of courses. I am thankful to Dr. Nolan Holland and Darlene for their continual support and making things very comfortable. Without your support, it would be really difficult to get through administrative things so easily.

I express thanks to my fellow lab mates in the Materials Research group for stimulating discussions. I am extremely grateful to my parents for their love, prayers, caring and sacrifices for educating and preparing me for my future. I am very much thankful to my new family David and Courtenay Cottenden for their love, understanding, prayers, and continuing support to complete my Masters in a completely new country. My Special thanks go to my best friend and family Abdul Mujeeb for the keen interest shown to complete this thesis successfully. Last but not the least, I would like to thank my brother Salman khan for being the constant source of inspiration throughout my life and believing in me. This accomplishment would have not been possible without them. Finally, I would like to thank NASA (Grant No. 80NSSC20K0736) for funding this project.

DEFECT AND DISORDER IN DENDRITIC ARRAYS SOLIDIFIED ON EARTH AND ON THE SPACE STATION

SHIRIN KHAN

ABSTRACT

Under a NASA (National Aeronautics and Space Administration)-ESA (European Space Agency) collaborative research project, MICAST (Microstructure formation in the casting of technical alloys under diffusive and magnetically controlled convection conditions), three Al-7wt% Si samples (MICAST-6, MICAST-7 and MICAST2-12) were directionally solidified at growth speeds varying from 10 to 50 μm s^{-1} aboard the International Space Station to determine the effect of mitigating convection on the primary dendrite array. The purpose of this research is to examine the ordering in the pattern formation during dendritic array growth of binary metallic alloys and explore if natural convection affects the extent of the disorder. Contrary to the expectations the MICAST samples also show some defects, such as misoriented primary dendrites or macrosegregation usually attributed to natural convection. It is observed that all of the primary dendrites on a cross-section do not have identical shape and morphology. Natural convection during terrestrial growth introduces more scatter in their morphology and distribution. Fast Fourier Transform analysis of the transverse images should be investigated as another tool to quantitatively determine the extent of disorder in the mushy-sone introduced by natural convection.

TABLE OF CONTENTS

Page

CHAPTER

LIST OF TABLES

Table Page

LIST OF FIGURES

Figure Page

CHAPTER I

INTRODUCTION

1.1 Directional Solidification

In directional solidification, process alloy is melted, and solidification starts from one end and goes on until the whole melt solidifies. It occurs in such a manner that molten metal feed is always available for that portion that is just solidifying[1]. This process is important because the microstructure is determined by processing conditions such as thermal gradient, growth speed, and the alloy physical properties such as solute content, phase diagram, etc. The most common microstructure is dendrite which is a tree-like structure.

One of the most important industrial applications of directional solidification is the production of superalloy turbine blades. The turbine blades rotate at high speed, so they are subjected to high combustion temperature. This produces creep deformation along grain boundaries which limits the blade life. The best solution to decrease such failure is to have the blade with a single grain, which is possible by directional solidification. Turbine blades are composed of nickel-based superalloys that are manufactured under constant thermal gradient G [K/cm] and growth speed R [cm/s]. During directional solidification, two types of grain microstructures are formed, columnar grains and equiaxed grains[2,3]

1.2 Mushy Zone Morphology

1.2.1 Dendrites

The typical mushy-zone, shown in Figure-1 for an alloy consists of arrays of “tree” like clusters, called primary dendrites. This primary dendrite tree trunk diameter increases from their tips in the vicinity of the all-liquid region to the eutectic temperature at the bottom of the mushy-zone. Such trees in Face Centered Cubic (FCC) alloys have orthogonal side-branches (secondary arms), and these side-branches have their orthogonal branches (tertiary arms) and so-on. Faster growth rate yields finer features and tighter packing and as a result smaller primary dendrite spacing. The dendrite spacing, trunk diameter, and branch spacing are all dependent on the growth conditions and physical properties of alloy[1-4].

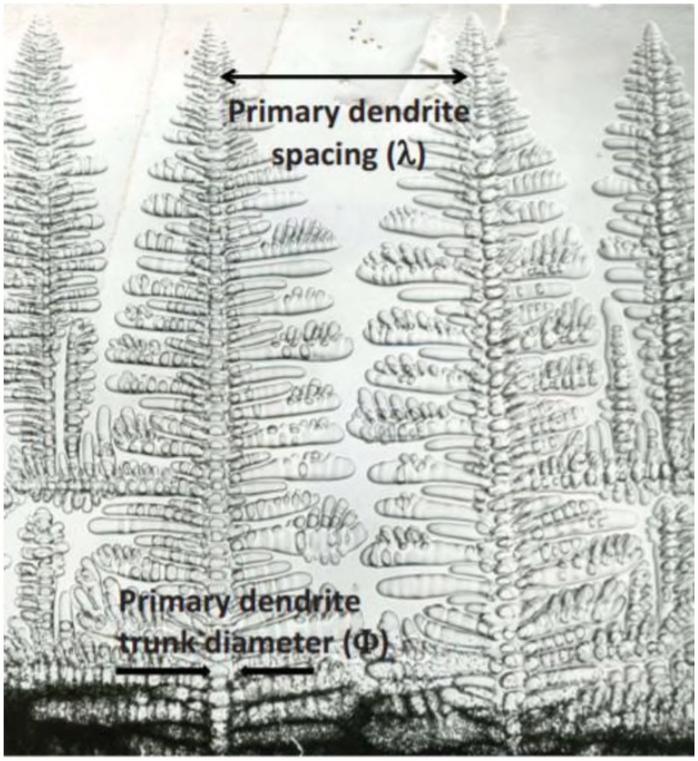

Figure 1. “Transparent alloy” directionally solidified (~ 5µm/s ,~30Kcm1) (Courtsey, Dr. Grugel, NASA-MSFC)

1.2.2 Eutectic

As the primary dendrite tips begin to form from the surrounding liquid the temperature drops below the alloy liquidus temperature (T_l) because of the curvature at the dendrite tip. As shown schematically in Fig. 3, the primary dendrite tip temperature (T_t) is slightly below (T_l) because of the curvature undercooling. Therefore, for alloys where the ratio of the solute content of the solid phase and the liquid in equilibrium 'k' (the solute partition coefficient) is less than one, at the array tips (Ct) the composition of the liquid is slightly higher than the nominal solute content of the alloy (Co)[4]. Since the diffusion coefficient of the solute in solid is at least two orders of magnitude slower than that in the liquid, further solidification of the primary dendrites results in continued solute enrichment of the inter-dendritic melt due to the solute continuously being rejected from the growing solid and getting accumulated in the inter-dendritic melt. In the end, the two-phase eutectic solid forms when the inter-dendritic melt [4,5] reaches the eutectic composition at the base of the dendrite arrays. Consequently, the inter-dendritic melt is solute rich at the base of the dendrite array and solute poor near the array tips[5].

Depending on whether the increasing solute results in increased melt density or results in the reduced melt density, the density of the inter-dendritic melt in the mushy-zone either increases downside or decreases downside during directional solidification process with melt on the top and the solid on the bottom. When the less dense melt is below, and the higher density melt above then natural convection driven by gravity can occur. Since the temperature gradient is stabilizing during directional solidification, convection in the mushy zone should depend only on the solute effects[6,7].

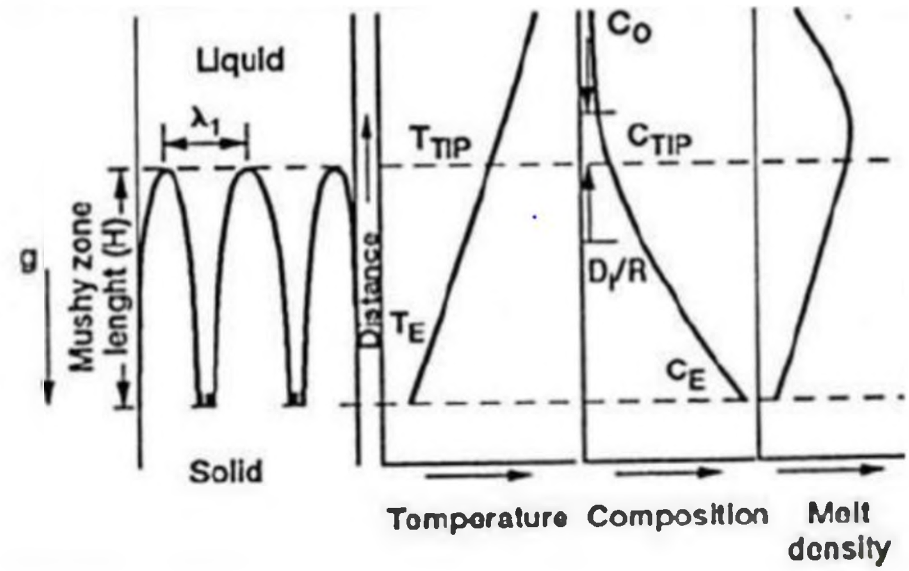

Figure 2. Schematic Temperature and Density Profiles in inter-dendritic Liquid[7]

1.3 Microgravity

Microgravity refers to a condition where the gravitational force is week. So why we need microgravity for directional solidification? Several types of research have been done to evaluate the relationship between primary dendrite arm spacing and the solidification processing parameters like thermal gradient, growth velocity, and alloy composition[7-16]. The theoretical models assume diffuse transport environment and the terrestrial experiments are invariably influenced by thermosolutal convection, therefore deviation of the experimental observations from theoretical predictions are simply attributed to the presence of convection during solidification[6-10]. It is now well known that thermosolutal convection of bulk components during DS cannot be eliminated during terrestrial DS irrespective of the alloy compositions selected.

Al-19% Cu alloys where solute enrichment increases melt density is seen, as shown in Fig. 2(a). The dendrites across the sample cross-section have non-uniformity (as shown in Fig. 3(a) [8] . Plume type of thermosolutal convection occurs in alloys where solute enrichment decreases melt density, as typically shown in Fig. 3(b)[7]. Notice the dark looking “freckle” defect on the top section of the image (b) in the microstructure. Hence, several experiments have been done in low gravity in space with the purpose of obtaining dendrite array morphology growing under diffusive transport conditions, i.e., having undergone solidification in the absence of convection in order to compare the observed microstructural features with predictions of the available theoretical models[17-19].

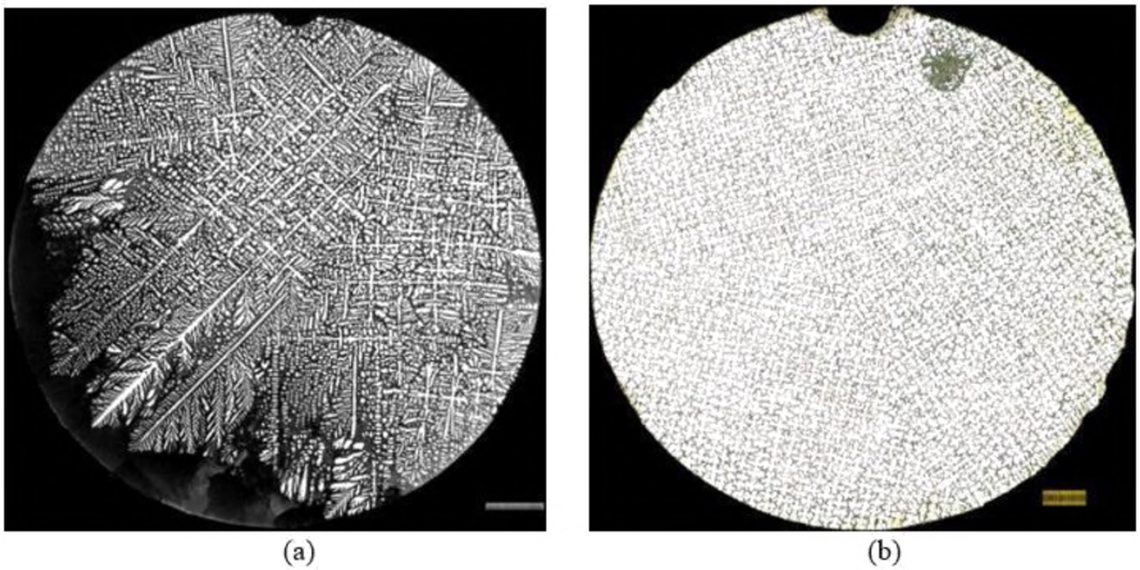

Figure 3. (a) Image of an Al-19 % Cu alloy transverse slice[8], grown at 10 μm s^{-1}. (b) Image of a Pb-6 % Sb alloy transverse slice[7], grown at 10 μm s^{-1}.

1.4 MICAST

Under a joint collaborative research project between NASA and European Space Agency (ESA), MICAST (microstructure formation in the casting of technical alloys under diffusive and magnetically controlled convection conditions) three Al-7% Si alloy samples directionally solidified in the Materials Processing Lab at Cleveland State University were remelted and directionally solidified on the International Space Station to examine the influence of natural convection on the dendritic array morphology As shown schematically in Fig.4, if the convection were not present, then remelting of the single crystal dendrite feedstock followed by its directional solidification would result in maintaining the same dendrite alignment along the entire sample length. Due to a lack of thermosolutal convection caused by gravity, it should also not produce any radial or longitudinal macro-segregation.

Primary dendrite spacing and primary dendrite trunk diameter were measured as a function of growth speed from the microstructures examined after the MICAST-samples were received at Cleveland State University. The results show a good agreement between the theoretically predicted spacings and trunk diameters [9,20] and the experimentally observed values from these three MICAST samples (MICAST-6, MICAST-7, and MICAST2-12). Although, after careful examination of the microstructures, "spurious grains" having dendrites that deviate from the orientation of the seed are observed in some of the MICAST samples [7], raising a possibility that convection may have been present in some of MICAST samples even though they were processed in the micro-g convection free environment of the Space Station.

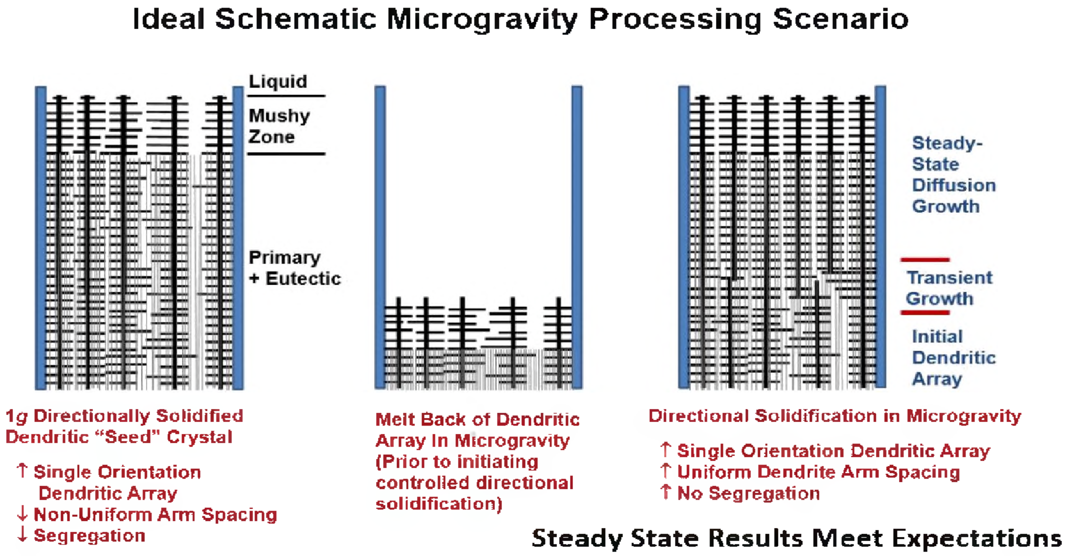

Figure 4. Directional Solidification results expected if conducted in Microgravity [Courtsey-Dr. Grugel (NASA-MSFC]

1.5 Misoriented Grains

The major cause of rejection of the single crystal gas-turbine blades manufactured by industry is the presence of spurious grains. The spurious grains are known to form in the presence of melt undercooling. However, it is not possible for the melt to undercool during directional solidification of alloys. Forced convection during directional solidification is known to result in misoriented grains. Depending on the density difference between the solid formed and the surrounding melt these broken fragments may rise, or sink. If they are not entrapped within the primary dendrites growing around them then they can grow into misoriented grains. The fragments can align themselves in any direction and therefore this new stray grain has a different orientation than the original solidified portion. Decelerating growth speed and melt back of bulk samples also can lead to the fragmentation of side-branches[21-24]. Another possibility is the fragmentation of sidearms via solutal-remelting caused by convection in the mushy-zone. If the liquid in the bottom of the mushy-zone which is solute-rich is forced to flow upwards, then it comes in contact with side-branches which formed at higher equilibrium temperatures. The solute rich melt then can remelt some of the branches and form fragments that can develop into spurious grains[21].

1.6 Purpose of This Research

As mentioned earlier the primary dendrite spacing and trunk diameter measured from the MICAST samples directionally solidified on the Space Station showed a good agreement with the theoretical models that assume diffusive transport [9,20] . However, the morphology and distribution of the primary dendrites on the sample cross-section do not appear to be uniform. Also, there are indications that convection may have been present during the processing of some of these MICAST samples. A cursory look at the MICAST transverse microstructure shows that all the dendrites do not have identical shape and morphology. Yet, no detailed study has been carried out to determine the extent of such non-uniformity and its dependence on natural convection. The purpose of this research is to examine the effect of processing parameters, especially growth under diffusive transport conditions vs. that in the presence of natural convection, on the primary dendrite array morphology and their uniformity. In this research three sets of microstructures have been examined for this purpose; (1) Al-7% Si alloy samples directionally solidified on the International Space Station (in micro-gravity condition) in absence of natural convection, (2) Al-7%Si alloy samples directionally solidified terrestrially in our lab at CSU, and (3) Al-3% Cu simulated dendrite arrays [25] (Numerical simulation assuming solute transport, no convection). Morphology details such as the orientation of secondary arms and variation in their orthogonality, length ratios of their orthogonal sidearms, the ratio of side-branch length have been quantitatively measured to accomplish this aim.

CHAPTER II

EXPERIMENTAL PROCEDURE

2.1 Directionally Solidified

Al-7Si alloy was melted in argon inert gas and poured into a copper mold to create cylindrical feed rod for subsequent terrestrial directional solidification in graphite crucibles (19 mm OD and 9.5 mm ID). Directional solidification was carried out by remelting these feed-rods under 10^{-4} torr vacuum and translating the graphite crucible away from the heat source at 20 μm s^{-1} under a thermal gradient of 40 K cm^{-1}. The process was used to create [100] oriented single crystal samples which were about 30-cm long. Cylinders of 24.5 cm long and 7.8 mm diameter were obtained by machining the [100] oriented samples and sent to the ESA where they were placed in Alumina crucibles having 12 thermocouples embedded on the alumina crucible surface. This thermocouple attached alumina crucible was then inserted into a Sample Cartridge Assembly (SCA). Three such SCAs were created and identified as MICAST-6, 7, and 12. The SCA schematically showed in Fig. 5(b) was used by astronauts on the Space Station. Low Gradient Furnace (LGF)[26] shown in Fig. 5(a) was used for directional solidification. This Bridgman-type furnace (LGF) is housed in a vacuum chamber (the polished circular door-like feature in NASA's Materials Science Research Rack (MSRR) view of the middle right) (Fig 6(a) and (b)). All the three samples of Al-7Si, MICAST-6, MICAST-7, and MICAST2-12, were directionally solidified in space at gravity levels below 10^{-4} g.

Initially, the sample was held stationary while the furnace was kept away from the SCA. The furnace was brought to an initial temperature and translated back to remelt 11 cm of the 25.4 cm long single-crystal feed rod so that the original dendrite orientation can be maintained. The thermal equilibrium was established by keeping the furnace stationary for MICAST-6 for 2 hours, and MICAST-7 and MICAST2-12 samples for less than 1 hour. As shown in Fig. 7 below during subsequent directional solidification the thermal gradients were approximately 18.5 K cm^{-1}, 24 K $\text{cm}^{-1,}$ and 26 K cm^{-1} for the MICAST-6, MICAST-7, and MICAST2-12 samples respectively. Growth speeds ranging from 5 $\mu\text{m s}^{-1}$ to 50 $\mu\text{m s}^{-1}$ were achieved using the three MICAST Sample Cartridge Assemblies. [20].

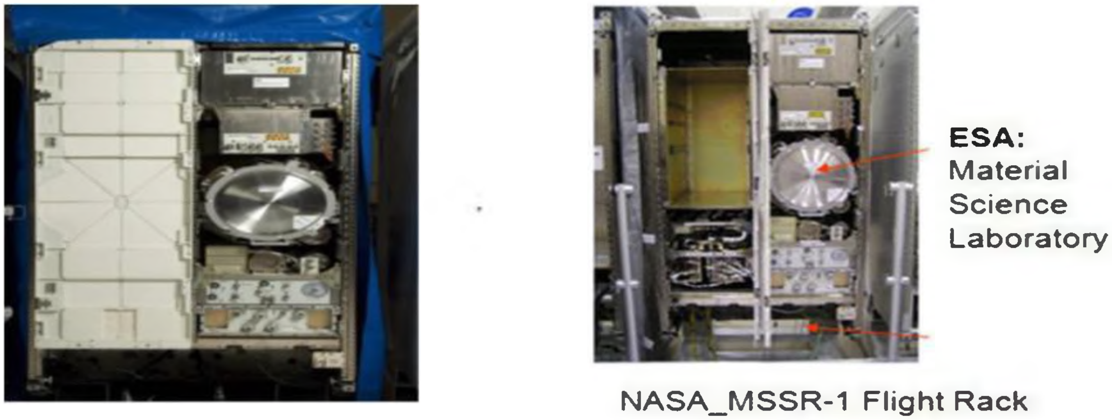

Figure 5. International Space Station Microgravity Science Research Facility[26].

(a) (b)

Figure 6. (a) ESA_MSL Low Gradient Furnace (LGF) used for the directional solidification and (b) Sample Cartridge Assembly (SCA), which includes a sample for an ISS directional solidification experiment[26]

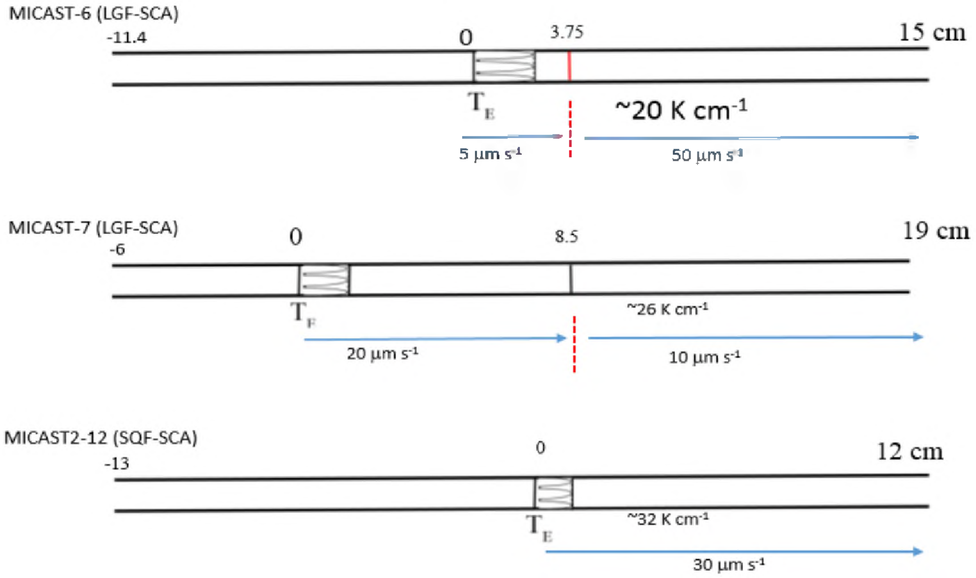

Figure 7. Processing conditions for MICAST-6, MICAST-7, and MICAST-2-12 samples during DS.

2.2 Cutting, Mounting, and Polishing

The directionally solidified MICAST samples were removed from the alumina crucible upon their return to NASA. X-ray radiography was conducted at several rotations on the sample while the samples were within the alumina crucible. The samples were then extracted from the alumina crucible and examined by metallography techniques. Thin slices were cut along the sample length for the examination of the dendrite array morphology on the transverse sections. The samples were mounted in a thermosetting epoxy resin. The mold cylinder and cap were greased with oil so that the sample can be removed easily. After the greasing, the sample was placed inside the mold. The epoxy resin was slowly mixed with hardener for 5 minutes and then poured in the mold over the sample. The samples were kept overnight for curing and after hardening, removed from the mold. Identification numbers were engraved on the samples. The abrasive grits of various grades were used to grind and polished the samples on Buehler's automatic grinder and polisher. Steps for grinding and polishing are shown in Table.1.

Table 1 Steps for Grinding and Polishing

Grade	Force/ Sample	Time (min)	RPM
400 (Grinding)	3 lbs	1	120
600 (Grinding)	3 lbs	1	120
800 (Polishing)	3 lbs	2	120
1200 (Polishing)	3 lbs	2	120
0.05μm (Fine polish)	4 lbs	8	120

An etching acid solution composed of 2 ml of each Hydrochloric and Hydro-fluoric acid added with 5 ml of Nitric acid, and then diluted with 190 ml of distilled water was used for some samples. The polished surface was then rubbed gently with the cotton swab soaking in etched solution for 5 to 10 seconds. The sample was then placed under the cold water stream.

2.3 Image Analysis

The optical images were taken at 50-X magnification with the help of HL Image++ 98 software. This image was taken in 60 to 70 small individual parts for a sample of the 9-mm diameter cross-section. These individual parts were then joined in a single montage using photoshop. The montaged images were then further analyzed using an open-source image analysis software 'ImageJ'. A small portion of a typical image is shown in Fig. 8.

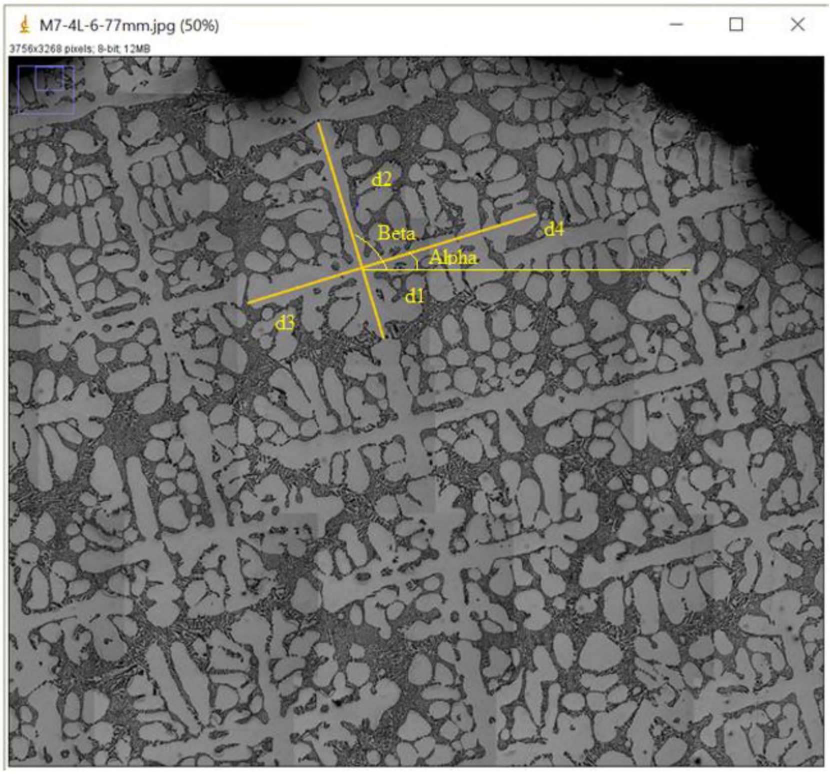

Figure 8. Image of a MICAST sample showing side arm d_1, d_2, d_3, and d_4 location in a dendrite along with angle alpha and beta.

2.3.1 Grain Orientation Analysis

Grain orientation analysis was carried out by measuring dendrite arm length. using ImageJ software in the following manner.

1. The image was open in ImageJ software and it was converted into a binary image.
2. The line-selection tool was selected, and a line was drawn between two endpoints of a dendrite arm. The line was marked from bottom to top and then left to right to avoid the negative angle measurement. The length was measured by selecting Analyze > Set Measurements >Bounding rectangle > OK. which measures a rectangle bounded by the two endpoints of lined’ acting as a diagonal.
3. As shown in figure 10 the bounding rectangle dimensions name BX, BY, Width, Height, Angle, and Length was printed, and it was saved in an excel file. ROI set (ROI: Region of Interest) was also measured and saved in a separate file.

When a line was drawn on the image the measurements provided by the application were in the form of bounding rectangle i.e. it gave as coordinates (*BX, BY*) of top-left point of the rectangle. The line drawn was treated as a diagonal of the rectangle as shown in figure 9. The bounding rectangle also includes measurement of height and width.

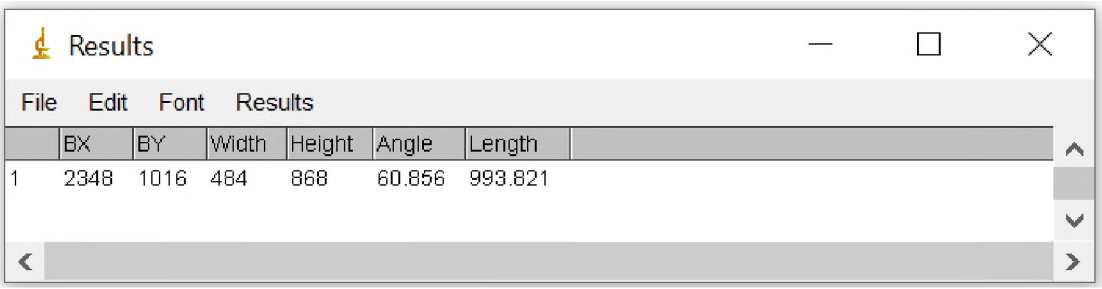

	BX	BY	Width	Height	Angle	Length
1	2348	1016	484	868	60.856	993.821

Figure 9. Window image shows a bounding rectangle measurement results extracted from a line drawn on the length of the arms of a dendrite.

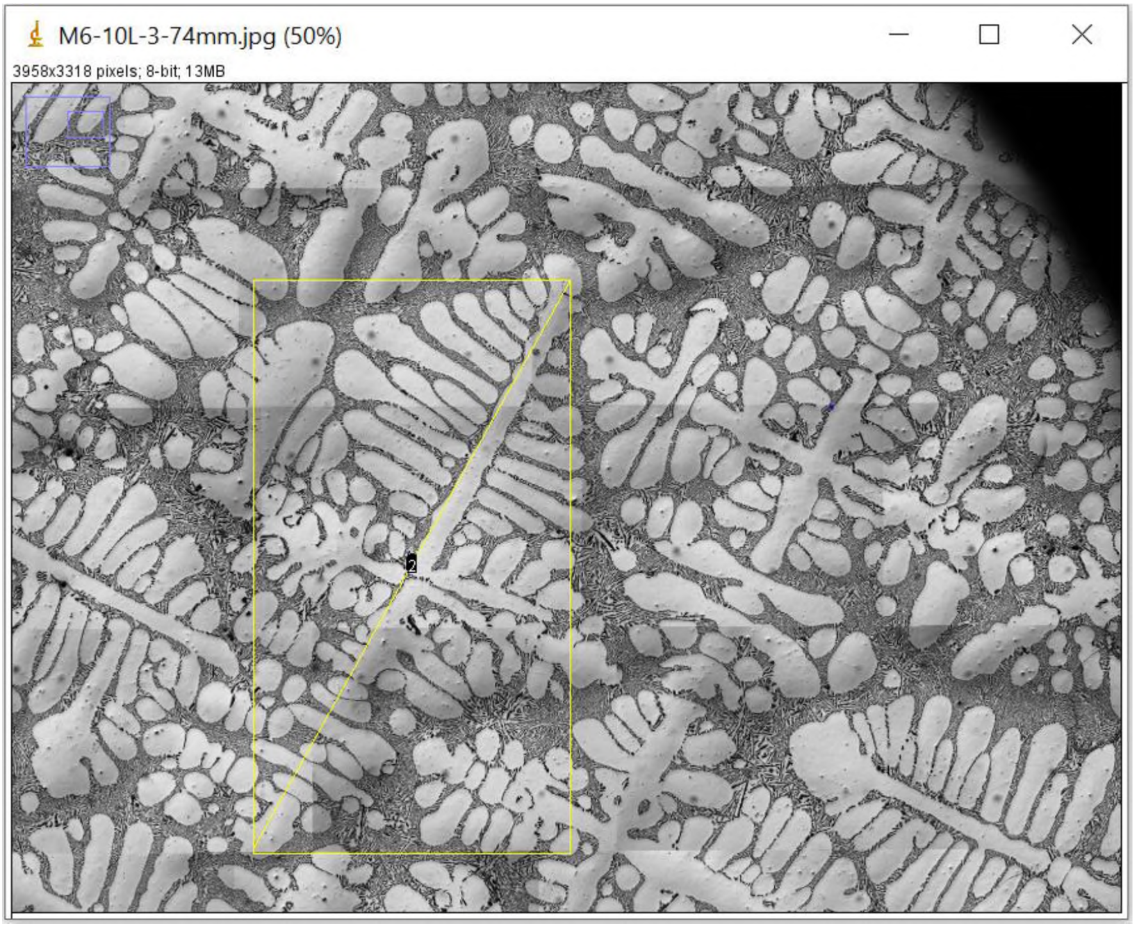

Figure 10. MICAST samples image shows a bounding rectangle measurement line drawn on the length of the arms of a dendrite.

2.3.2 Data Analysis Using MATLAB Code.

The bounding rectangle dimensions were then run through MATLAB code to find the dimensions of sidearms and angles. Three different types of MATLAB codes were formulated to extract the required data from image analysis.

2.3.2.1 Arm Length Analysis

The first MATLAB code was designed to calculate the length of the sidearms. It is formulated in such a way that it provides us the length of all the four side-arm of each dendrite irrespective of their angle of rotation (α and β). This is calculated with the help of the coordinates and the point of intersection of the lines.

The MATLAB code is explained in detail as follows:

1. The code first took the result excel file as an input and stored it in the form of a matrix. The numerical values of the excel file were sat in a matrix called raw (r) was the number of rows and (c) was the number of columns in data excel file.
2. Several 'for' loop was made which scanned pairs of the line in the "raw" matrix for (n=1: (r/2)) this if takes care of the regular drawn lines. The sixth element of each row was the angle and the decision about the use of BX and BY as a known point on the drawn line was based on that angle value.
3. The loop determined the intersection point of the line in the form of coordinates and using this intersection coordinates dendrite sidearm length was resolved.
4. With the help of sidearm length, the sidearm ratio, sidearm anisotropy, and the difference between alpha and beta were concluded.
5. After finalizing all the arithmetic, an output file was generated to present all the results.

2.3.2.2 Angle Sorting

This MATLAB code was written to design the graph which can help us in finding the range of dendrite grain. This graph shows the number of angles belongs to a range by review the result excel file. The code takes the excel file as input in a similar way as the *Arm length analysis* MATLAB code took. The numerical values of the excel file were sat in a matrix called raw (r) was the number of rows and (c) was the number of columns in data excel file, raw sorted based on the row (6) i.e. angles using bins which were 2 deg wide. Histogram plot was created using this angle value. The figure below shows the resulting graph which was an output of this graph.

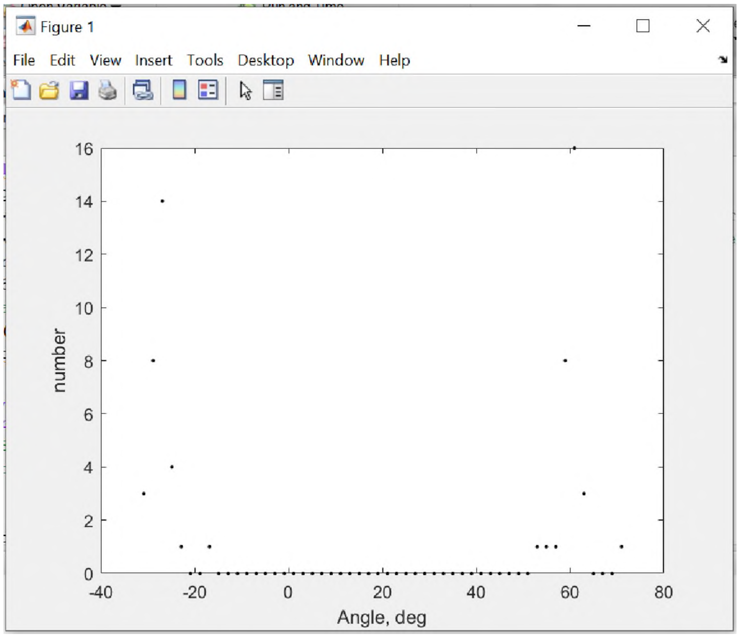

Figure 11. The image shows the histogram plot of the frequency of the angle of the dendrite arm.

2.3.2.3 Draw Lines

The third code was drafted to produce an imprint of the cross made for the measurement of the dendrite. Following steps were taken to produce the code for the cross plot:

1. An excel file was selected as an input. The excel file to be used as an input was the output excel file from the arm length analysis MATLAB code.
2. Similarly, the numerical values of the excel file were sat in a matrix called raw (r) was the number of rows and (c) was the number of columns in data excel file.
3. A loop was created to model the line using the coordinates. The loop differentiated the grain on the basis of their angle. A range of angles was defined inside the loop, which gives output crosses in the graph with the same color. This range of angle was gain from a histogram plot of angle sorting MATLAB code; else one could set the range by careful observation of the angle value from results.

4. If the second grain was present, then the second loop needed to be developed in the same MATLAB program. The different color was used for grain with different orientation as shown in figure

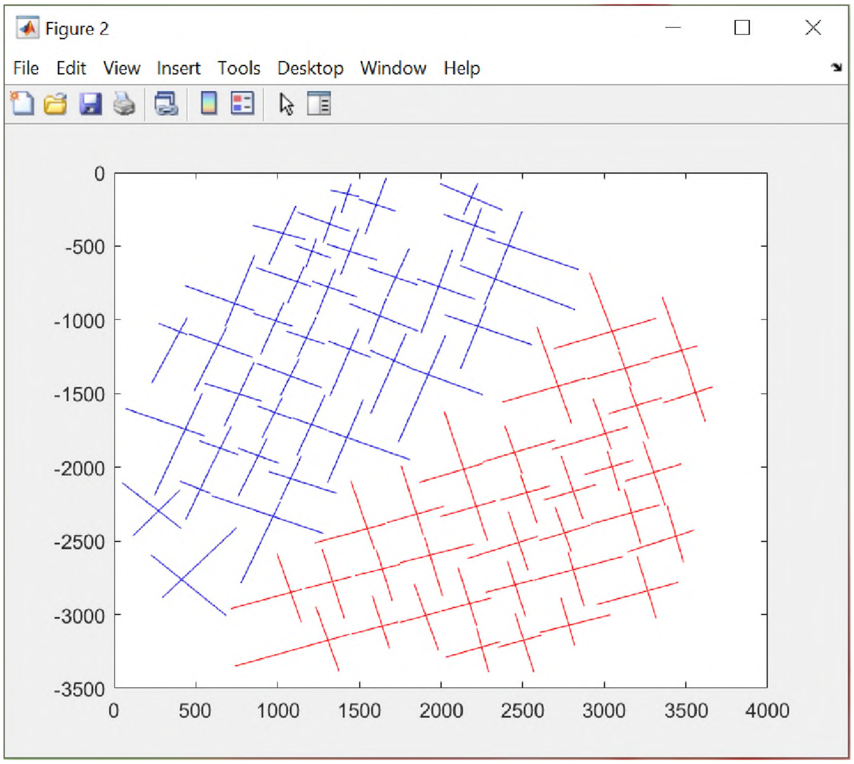

Figure 12. MATLAB graph showing dendrite side-arm.

CHAPTER III

RESULTS AND DISCUSSION

Effect of processing parameters, especially growth under diffusive transport conditions vs. in the presence of natural convection, on the primary dendrite array morphology and order, has been studied here. Three sets of microstructures have been examined; (1) Al-7% Si alloy samples directionally solidified on the International Space Station (in micro-gravity condition) in absence of natural convection, (2) Al-7%Si alloy samples directionally solidified terrestrially in our lab at CSU, and (3) Al-3% Cu simulated dendrite arrays (Numerical simulation assuming solute transport, no convection)[25]. Section 4.1 presents the transverse views of these three sets of dendrites. Section 4.2 presents a detailed characterization of these microstructures in terms of grain orientations (side-branch orientation distributions, and their deviation from the [100] orthogonality), side-branch length ratios, and their anisotropy. Section 4.3 presents a quantitative comparison of these parameters among the three groups of dendrite arrays and finally, in section 4.4 preliminary results from Fast Fourier transform (FFT) analysis of these microstructures are presented.

3.1 MICAST Samples (Microgravity)

From MICAST 6, 7, and 12 series, 5 samples are used to analyze misorientation. Figure 13 shows the transverse views along the directionally solidified length of the 5-microgravity processed Al-7%Si samples examined in this study. Table-2 lists their locations along the directionally solidified length and the growth conditions (thermal gradients and growth speeds)[7]. Fig. 13(a) through (e) are in the increasing order of the solidification growth speed, from 5.6 to 50 μms^{-1}. Fig. 13(a) and (e) are from MICAST-6 (5 and 50 μms^{-1}), Fig. 13(b) and (c) are from MICAST-7 (20 and 10 μms^{-1}) and Fig. 13(d) is from MICAST-12 (40 μms^{-1}) series. The corresponding ID and the locations of the transverse sections relative to the initial location of the Eutectic isotherm in the sample, and the corresponding growth speed and the thermal gradients in the liquid (G_l) and the mushy zone (G_m) at those locations during directional solidification are shown in Table-2.

Sample M6-8L-3 with growth speed of 5 μms^{-1} is showing evidence of steepling convection (notice the much longer side-arms in the top quarter of the figure) while the other 4 samples do not show this (Fig. 13 (b) to (e)). The number of dendrites seen on the cross-section is increasing as the growth speed increases. As the growth speed increases the randomness in the orientation of dendrites appears to decrease. Sample M12-T5 and M6-10L-3 with growth speed 40 and 50 μms^{-1} have the most aligned dendrites. Samples M6-8L3 and M12-T5 have two grains whereas others have a single grain.

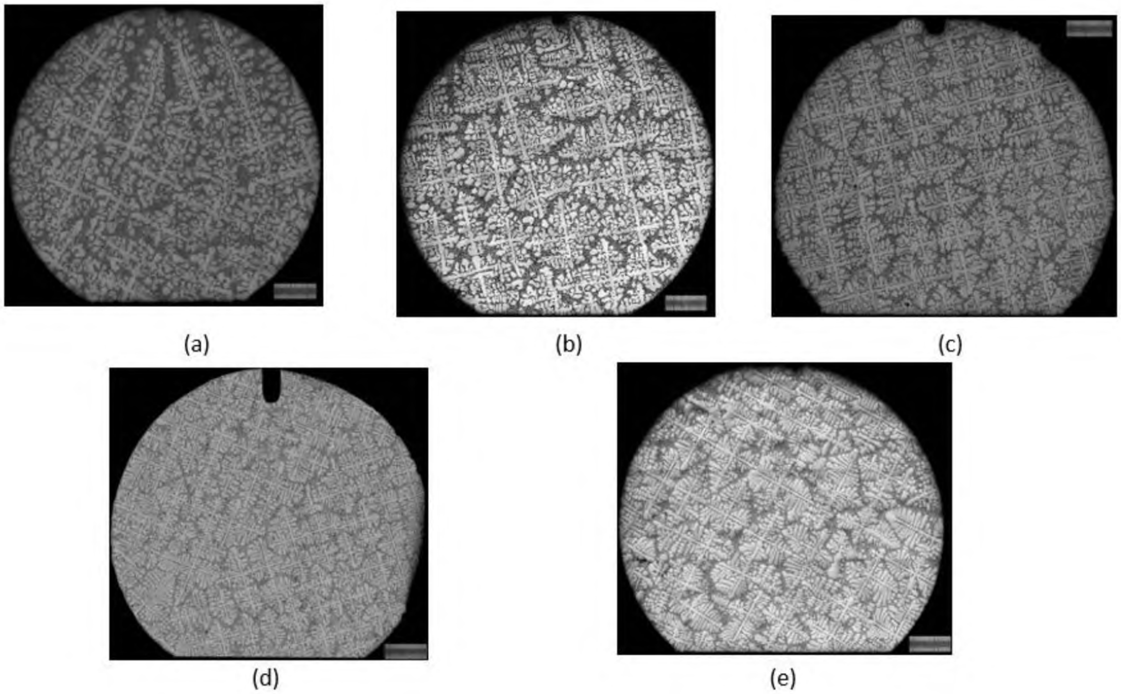

Figure 13. The transverse views of MICAST samples obtained from the space station (a) M6-8L-3 (b)M7-5L2-1 (c) M7-4L-6 (d) M12-T5 (e) M6-10L-3

Table 2 Growth Conditions and Sample Location for MICAST

Sample ID	**Distance from the Eutectic Isotherm (mm)**	**Velocity (μms^{-1})**	**Gl (K/cm)**	**Gm (K/cm)**
M6-8L-3	45	5.6	22.2	20.1
M7-5L2-1	127	10.8	25.9	23.7
M7-4L-6	77	21.2	26.7	24.3
M12-T5	69	40	32.8	32
M6-10L-3	74	50	19.8	18.2

3.2 MICAST-G Samples (Terrestrial Samples)

The samples having an initial aligned dendritic array that are prepared in the lab are designated as MICAST-G or terrestrial samples. These samples were prepared in solidification processing conditions nearly similar to the corresponding microgravity samples, especially the growth speeds. From MICAST-G series, again 5 samples were taken and analyzed. Table-3 shows the process conditions like growth speed and the thermal gradients during the directional solidification of terrestrial samples. The corresponding ID and the locations of the transverse sections relative to the initial Eutectic isotherm in the sample are also shown in the table. These samples are also arranged in the increasing order of the growth speed from 5 to 50 μms^{-1}.

Fig. 14 shows the transverse views along the directionally solidified length of the MICAST-G samples. The samples are arranged in the increasing order of the growth speed from 5 to 50 μms^{-1}. It is observed from the figure, that the number of dendrites is increasing as the growth speed is increasing and the dendrites are getting more aligned but the 5th sample with sample ID M6G-10L-2 with growth speed 50 μms^{-1} have less and unidentical dendrites.

Sample M6G-7T and M6G-10L-2 are showing severe steepling convection which results in extensive radial macrosegregation (notice almost 100% eutectic regions in the right-top quadrant of the cross-sections), Fig. 14 (a) and (d). The dendrites in these two samples are non-uniformly distributed, unlike the ordered distribution in M7G-5L1-4, M7G-4L-3, and Al-Si-3-25-15-6 samples. Sample M7G-4L-3 with growth speed 40 μms^{-1} appears to have 2-grains.

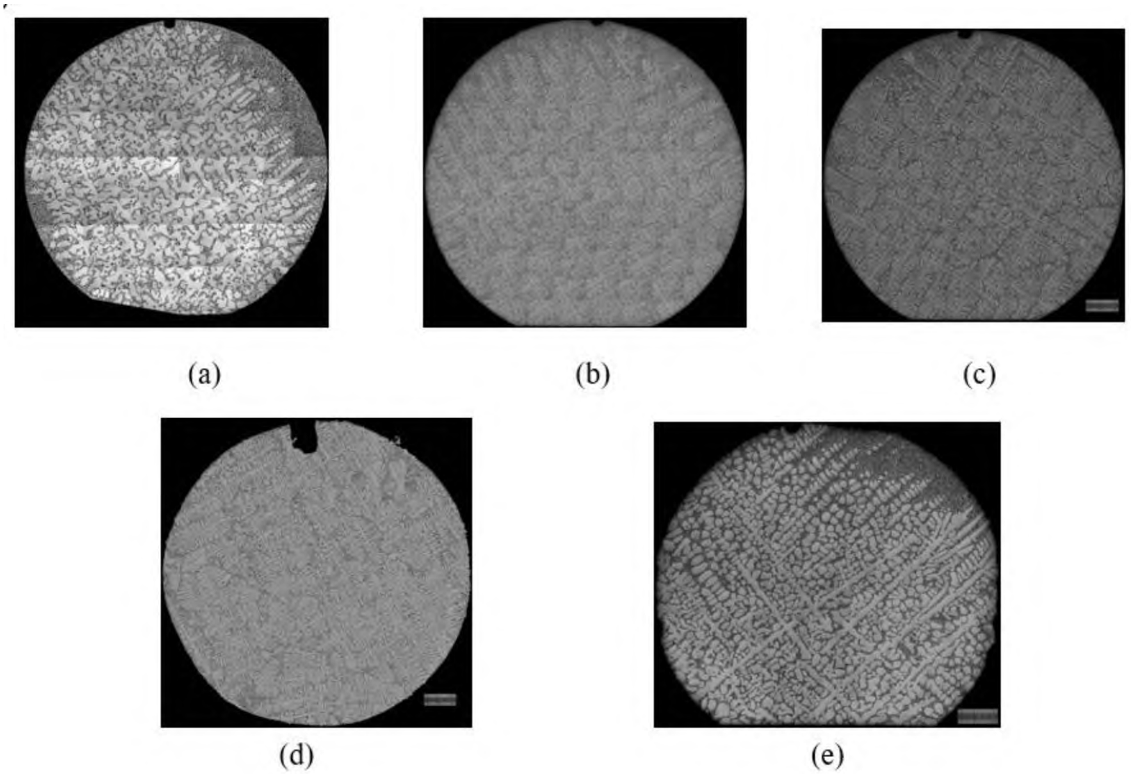

(a) (b) (c) (d) (e)

Figure 14. The transverse images of MICAST-G samples solidified terrestrially in the lab (a) M6G-7T (b) M7G-5L1-4 (c) M7G-4L-3 (d) Al-Si-3-25-15-6 (e) M6G-10L-2

Table 3 Growth Conditions and Sample Location for MICAST-G

Sample ID	**Distance from the Eutectic Isotherm (mm)**	**Velocity (μms^{-1})**	**Gl (K/cm)**	**Gm (K/cm)**
M6G-7T	30	5	15	21
M7G-5L1-4	132	10	25	29
M7G-4L-3	74	20	25	27
Al-Si-3-25-15-6	8	40	22.6	39.7
M6G-10L-2	71	50	15	21

3.3 Simulated Dendrites (From Theoretical Model)

A large-scale phase-field numerical simulation was performed to examine the initiation and growth of primary dendrite arrays formed during directional solidification of a single-crystal binary alloy by researchers at the Tokyo Institute of Technology using the graphical processing unit (GPU) supercomputer TSUBAME2.5[25]. This is the only simulated dendrite array study available in the literature because the three-dimensional simulation of primary dendrite array growing in a binary alloy is extremely computation-intensive. The simulation also assumed that only diffusive thermal and solutal mass transports were present and neglected convection in its analysis.

Six directional solidification simulations were performed for six different temperature gradients (G) under a constant pulling velocity (Vp) 100 μms^{-1} as shown in Table 4. These six simulation samples cover the array shapes varying from the unbranched cells to the dendrites having the orthogonal side-branches. Fig. 15 (a) to (e) shows the transverse views of the simulated dendrite arrays. The samples are arranged in the increasing order of the temperature gradient from 5 to 100 K/cm. The first sample Dend_1 has uniformly arranged dendrites with sidearms. As the temperature gradient increases the dendrites become less branched and their inter-dendritic-spacing decreases[26].

Table 4 Growth Conditions simulated dendrite

Sample ID	**Velocity (μms^{-1})**	**Gm (K/cm)**
Dend_1	100	5
Dend_2	100	10
Dend_3	100	20
Dend_4	100	50
Dend_5	100	100

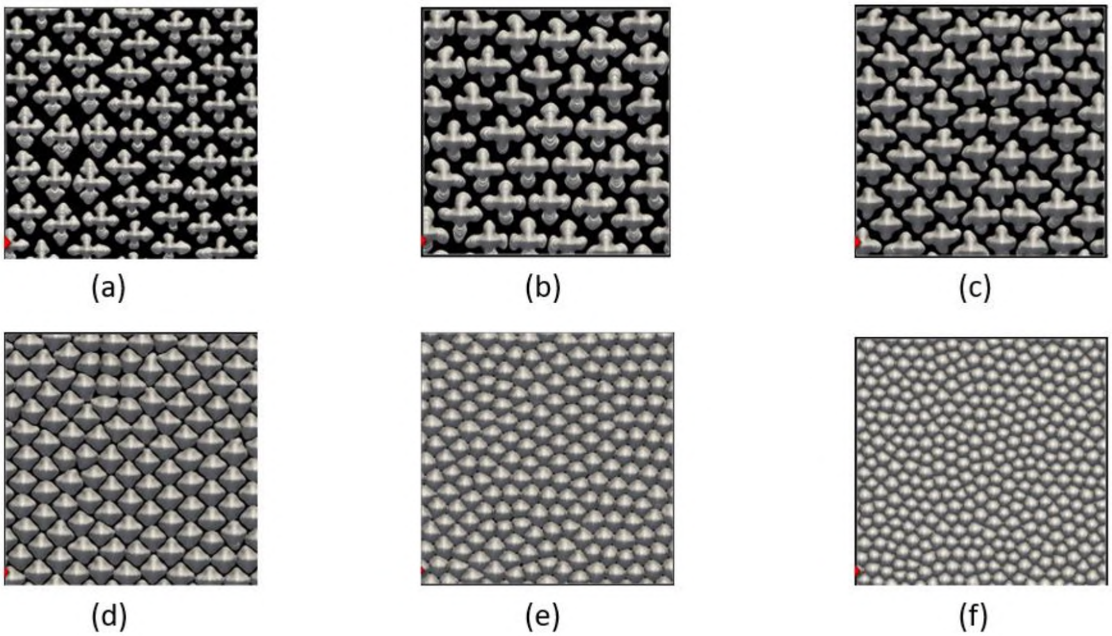

Figure 15. The transverse views of numerically simulated dendrite arrays (a) Dend_1 (b) Dend_2 (c) Dend_3 (d) Dend_4 (e) Dend_5 (f) Dend_6

3.4 Microstructure Evaluation Using Graphical Method

3.4.1 Frequency Distribution of Angles

In an ideal dendritic array of a face-centered-cubic alloy growing in [100] direction under only the purely diffusive solutal and thermal transports, the side-branches are expected to be orthogonal to each other, because they would also grow along <100> directions. The angles, α, and β, (described earlier in Section) were measured for all the microstructures examined in this study in order to examine the deviation from this ideality. Frequency distribution of angles α and β, are plotted in Figures 16, 17, and 18 for the MICAST, MICAST-G, and simulated dendrite samples, respectively. The y-axis of the graphs shows the number of dendrites belonging to a particular range of angles shown on the x-axis. These graphs were generated by using *Angle Sorting* MATLAB code written for this purpose. The width and height of the peaks are determined by a sigmoidal fit to the data by using the MATLAB software app. The peak width and height values are used in further analysis.

Fig. 16 (b), (c), and (e) show the presence of two peaks, the angles α and β located approximately 90 degrees apart from each other. This is an indication that these samples are single crystal, i.e., they contain only one grain. Fig. 16 (a) and (d) indicate the presence of four different peaks, indicating two sets of α and β being present. This indicates that these samples contained two grains, having different orientations. With increasing growth speed the peaks appear to be sharper indicating decreasing scatter in the orientation distribution of side-branches. It is interesting to note that the samples grown in the convection-free environment of space station do have significant scatter in the side-arm orientation, primary dendrites are not fully aligned and ordered as was expected.

The earth-grown samples (Fig. 17 (a) through (e)) show a behavior similar to the Space-Station processed samples. The scatter in the side-arm orientation is not significantly higher than the Space-Station processed samples. The numerically simulated dendrite array with side-branches (Fig. 18(a)) does appear to show only two peaks (single grain) and less scatter than the MICAST (Fig. 16) and MICAST-G (Fig. 17) samples.

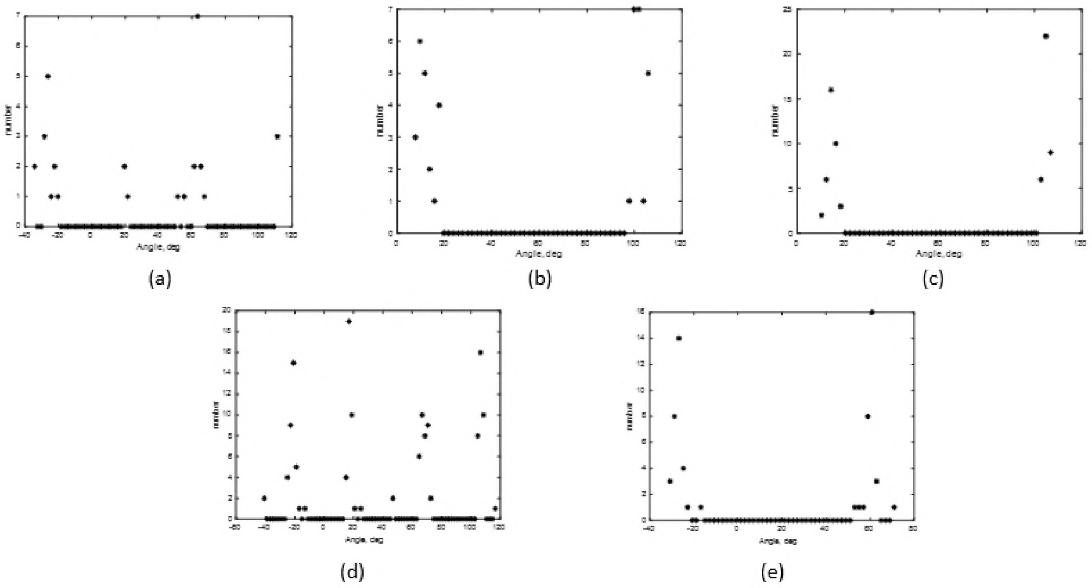

(a) (b) (c)

(d) (e)

Figure 16. Frequency distribution of α and β angles of MICAST samples generated using Angle Sorting MATLAB code (a) M6-8L-3 (b) M7-5L2-1 (c) M7-4L-6 (d) M12-T5 (e) M6-10L-3

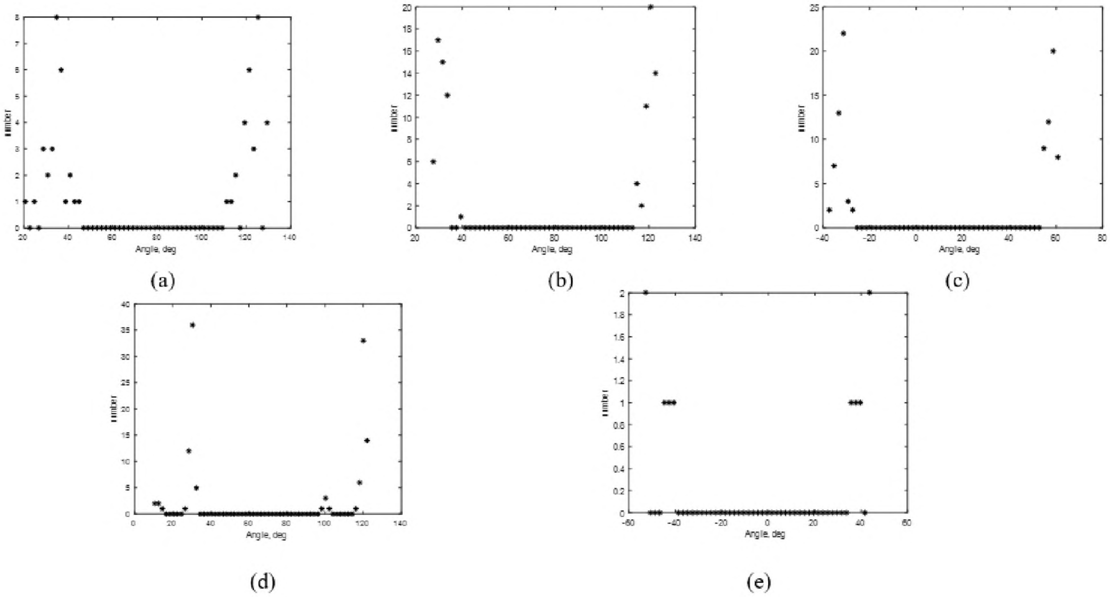

(a) (b) (c)

(d) (e)

Figure 17. Frequency distribution of α and β angles of MICAST-G samples generated using Angle Sorting MATLAB code (a) M6G-7T (b) M7G-5L1-4 (c) M7G-4L-3 (d) Al-Si-3-25-15-6 (e) M6G-10L-2

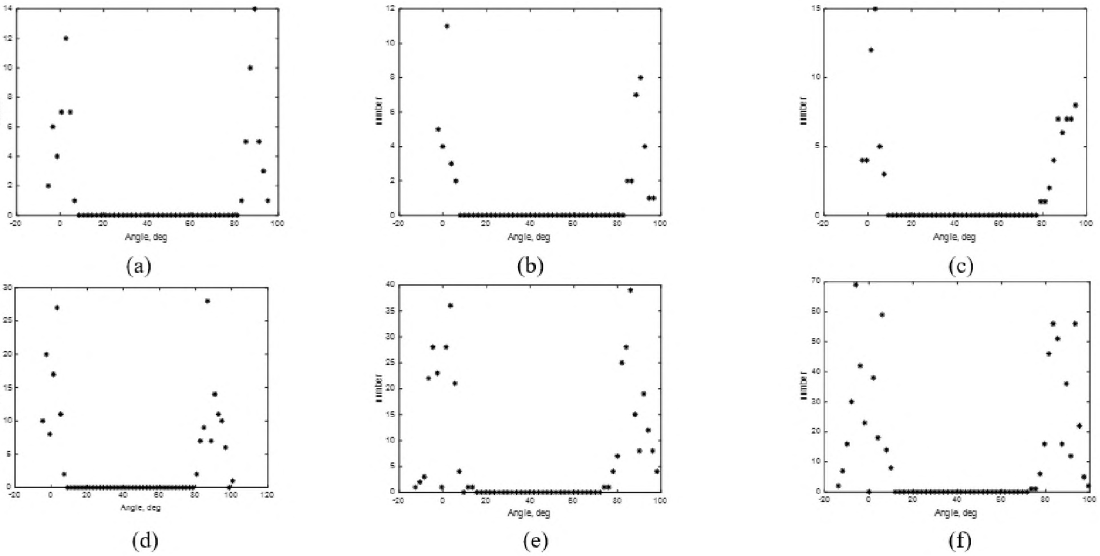

(a) (b) (c)
(d) (e) (f)

Figure 18. Frequency distribution of α and β angles of simulated dendrite arrays generated using Angle Sorting MATLAB code (a) Dend_1 (b) Dend_2 (c) Dend_3 (d) Dend_4 (e) Dend_5 (f) Dend_6

3.4.2 Side-Branch Anisotropy

The opposite side-branches in an "ideal" dendrite array growing under diffusive transport conditions, without any external disturbance, should be of equal length. Deviation of these ratios from unity is thus an indication of the side-branch anisotropy. Fig. 19 (a) shows a typical picture of a dendrite marked with d_1, d_2, d_3, and d_4 along with their corresponding angles, α and β. Fig. 19 (b) to (f), 20 (a) to (e), and 21 (a) to (f) plot d_1/d_2 and d_3/d_4 for MICAST, MICAST-G, and Simulated Dendrites Samples respectively. The side-branches d_1 and d_2 are opposite to each other along with the α angles and are therefore plotted as a function of α. The side-branches d_3 and d_4 are opposite to each other along with the β angles, hence they are plotted as a function of β. Some samples have two peaks of the same color, indicating the presence of 2-grain orientations in the same sample.

As shown in Fig. 19 (b), sample M6-8L-3 have dendrites with an opposite side-branch ratio up to 8, and angles α and β have more scatter. For the MICAST samples (Fg. 19) as the growth speed increases, the scatter in the α and β angles decreases indicating improved dendrite alignment. The maximum values of the d_1/d_2 and d_3/d_4 also appear to decrease as growth speed increases, indicating the development of more ordered morphology distribution, i.e, decreasing side-branch anisotropy. However, these ratios are still larger than 1. For MICAST-G samples, the scatter in the α and β angles also decreases as the growth speed increases (Fig. 20). However, there is no systematic decrease in the largest d_1/d_2 and d_3/d_4 ratios observed in the samples with the increasing growth speed as was seen in MICAST samples. It is interesting to note that the MICAST samples appear to have larger d_1/d_2 or d_3/d_4 values as compared with the MICAST-G samples. The simulated dendrite array with developed side-branches (Fig. 21(a)) has the d_1/d_2 and d_3/d_4 values much closer to unity. In addition the scatter in these values is significantly less as compared with MICAST or MICAST-G samples.

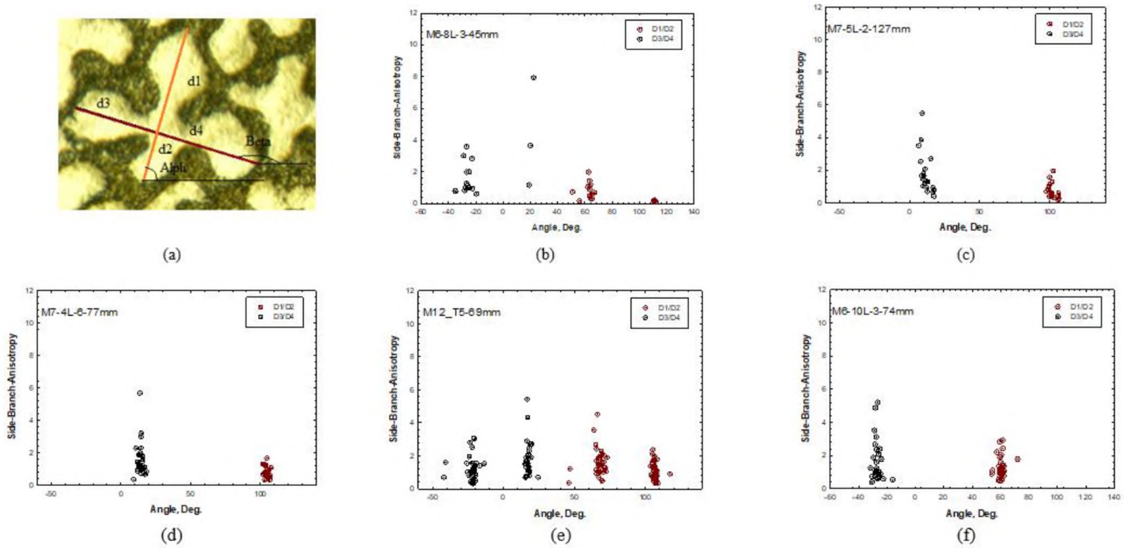

(a) (b) (c)

(d) (e) (f)

Figure 19.The ratio of the side-branches opposite to each other versus α and β angles of MICAST samples (a) Dendrite (b) M6-8L-3 (c) M7-5L2-1 (d) M7-4L-6 (e) M12-T5 (f) M6-10L-3

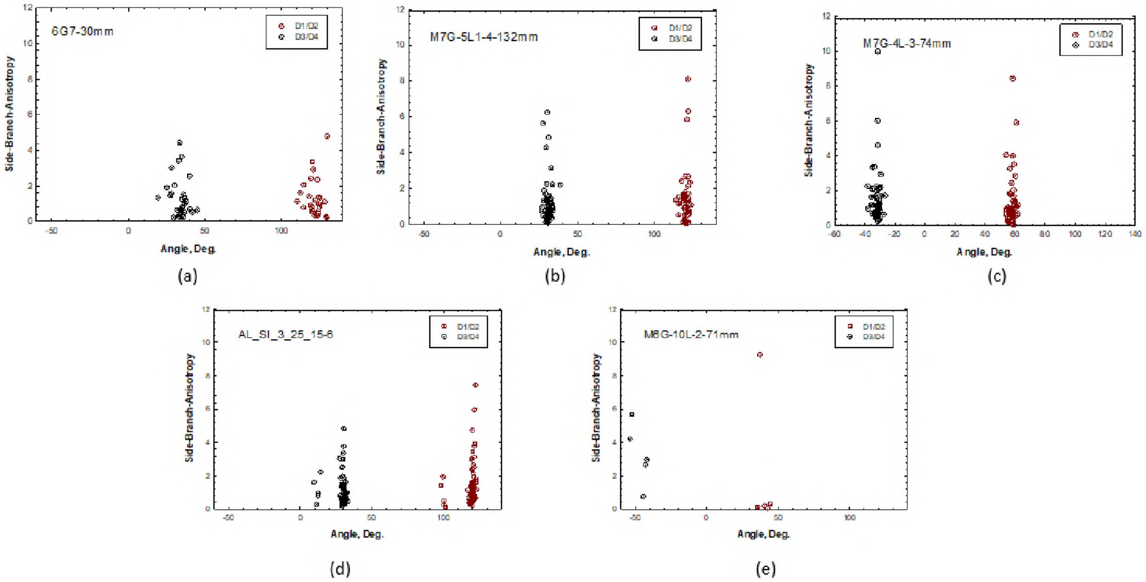

Figure 20.The ratio of the side-branches opposite to each other versus α and β angles of MICAST-G samples (a) M6G-7T (b) M7G-5L1-4 (c) M7G-4L-3 (d) Al-Si-3-25-15-6 (e) M6G-10L-2

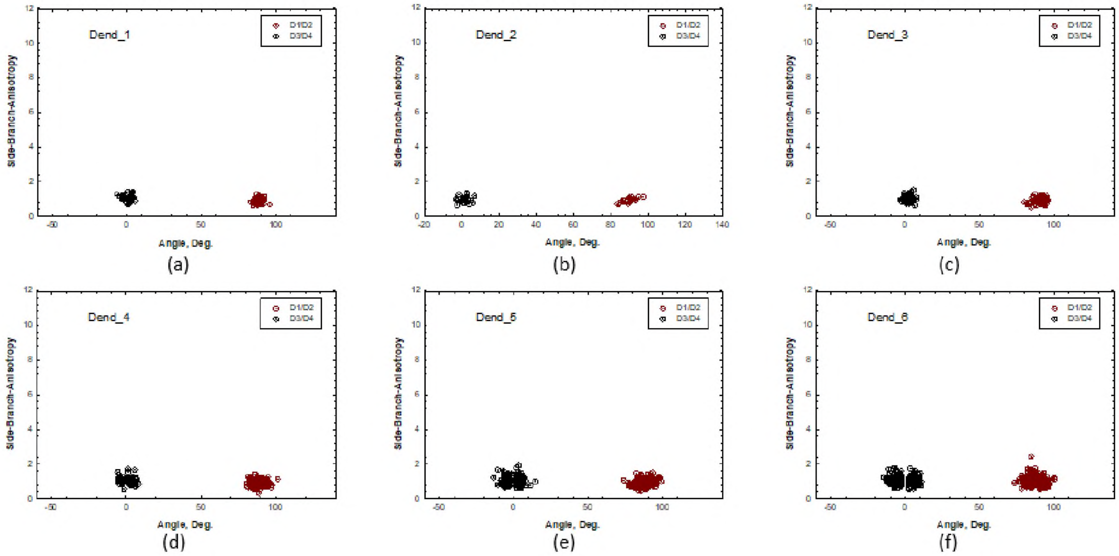

Figure 21.The ratio of the side-branches opposite to each other versus α and β angles of simulated dendrite arrays (a) Dend_1 (b) Dend_2 (c) Dend_3 (d) Dend_4 (e) Dend_5 (f) Dend_6

3.4.3 Side-Arm Ratio

The orthogonal side-arms in an "ideal" dendrite array growing under diffusive transport conditions, without any external disturbance, should be of equal length. Fig. 22 (a) shows a typical picture of a dendrite marked with the two orthogonal side-branches L_1, and L_2 crossing each other at approximately 90° along with angles α and β . Deviation of L_1/L_2 from unity would indicate that the primary dendrite trees in an array may not be arranged in a perfectly square pattern, but the distance between adjacent trees may be longer along one [100] direction than its counterpart [100], i.e., the side arms may systematical be preferring to grow longer along with one orientation. Fig. 22 (b) to (f), 23 (a) to (e), and 24 (a) to (f) shows the side-arm ratio (L_1/L_2) plotted against the angle α of MICAST, MICAST-G, and Simulated Dendrites arrays respectively.

Fig. 22 shows that the L_1/L_2 ratio of MICAST samples has a large scatter, values varying from one to as much as 4. The L_1/L_2 also appears to be always larger than unity. The scatter in the side-arm ratio appears to decrease with increasing speed. As the growth speed increases the primary dendrite trees not only grow closer to each other (interdendritic spacing decreases) they also appear to develop more uniform morphology trees. MICAST-G samples (Fig. 23) also show a similar pattern. The simulated dendrite array with side branches (Fig 24(a)) this secondary arm (side-arm) ratio to be closer to unity having least scatter.

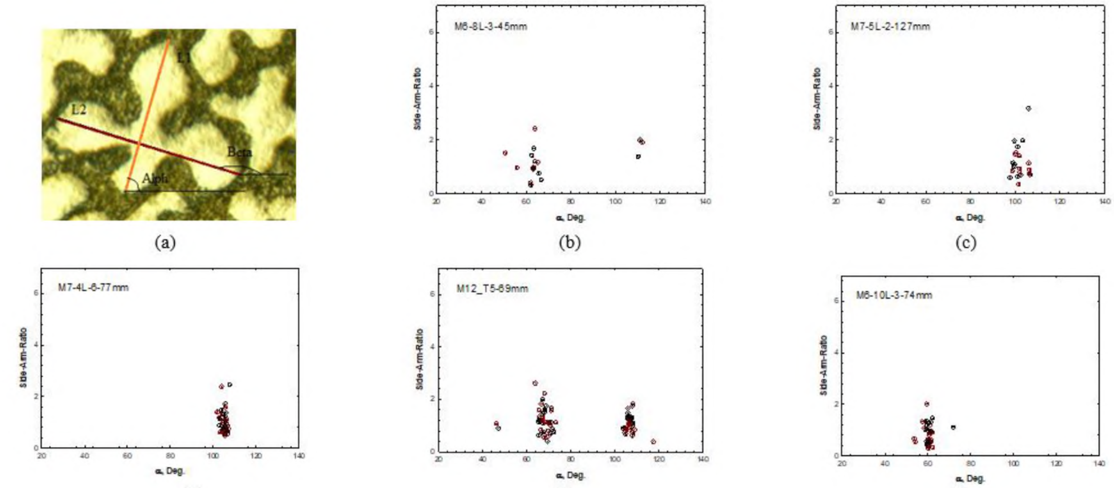

(a) (b) (c)

(d) (e) (f)

Figure 22.The ratio of side-arm length ratio versus α angles of MICAST samples (a) Dendrite (b) M6-8L-3 (c) M7-5L2-1 (d) M7-4L-6 (e) M12-T5 (f) M6-10L-3

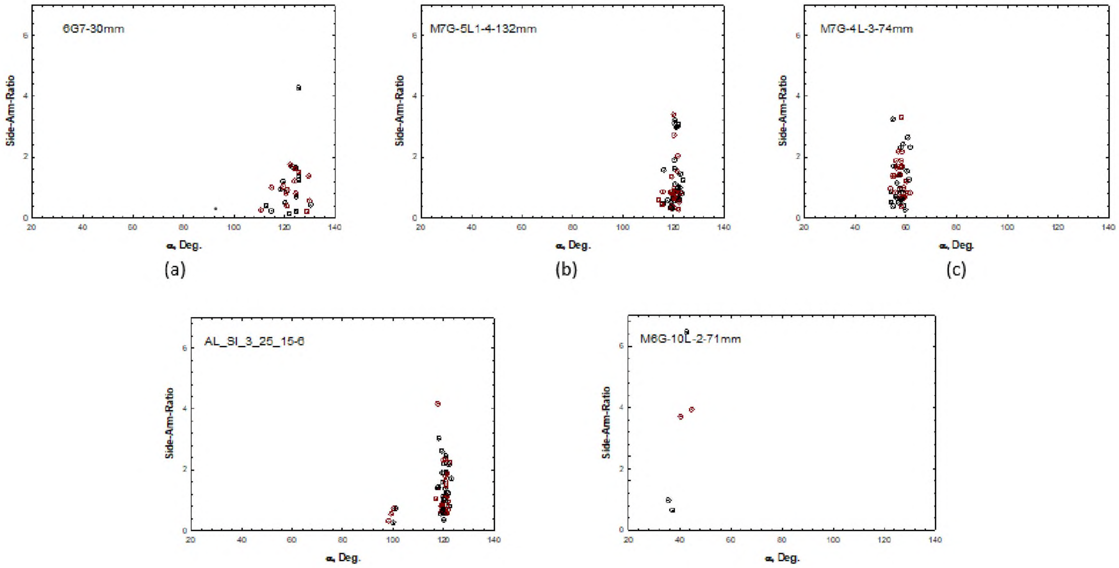

(a) (b) (c)

(d) (e)

Figure 23. The ratio of side-arm length ratio versus α angles of MICAST-G samples (a) M6G-7T (b) M7G-5L1-4 (c) M7G-4L-3 (d) Al-Si-3-25-15-6 (e) M6G-10L-2

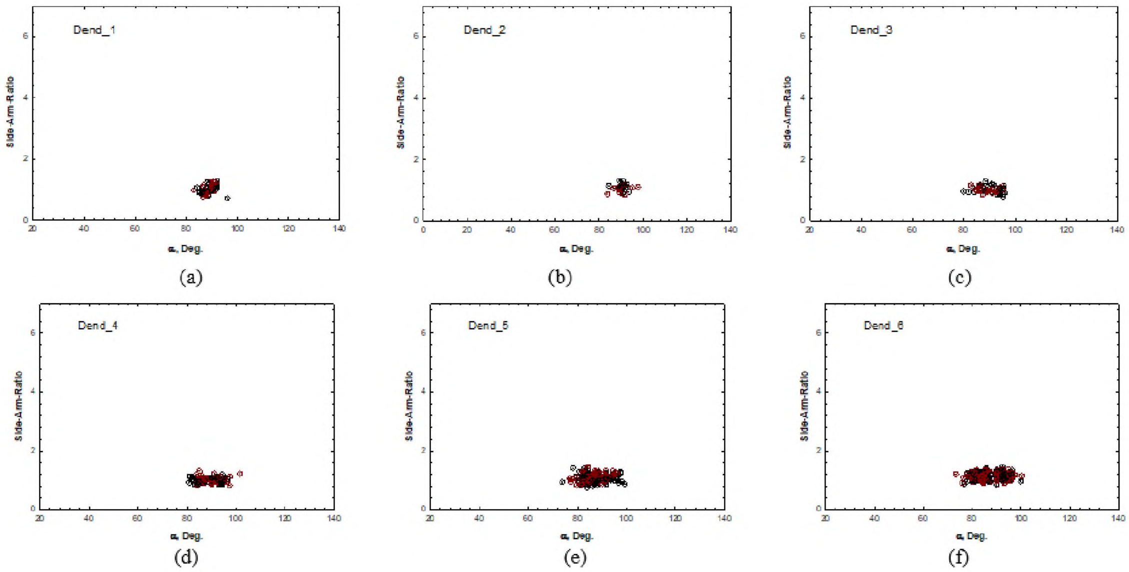

(a) (b) (c) (d) (e) (f)

Figure 24. The ratio of side-arm length ratio versus α angles of simulated dendrite arrays (a) Dend_1 (b) Dend_2 (c) Dend_3 (d) Dend_4 (e) Dend_5 (f) Dend_6

3.4.4 Magnitude of (alpha - beta)

Since the four side arms are expected to grow along the four orthogonal <100> crystallographic directions the difference between the α and β angles (Fig. 25(a)) is expected to be 90°. Deviation of (α - β) magnitude from 90° is an indicator of the non-uniform morphology distribution of primary dendrites growing in the same array. Dendrites having |α–β| very different from 90° indicate the presence of "misoriented dendrites" or "spurious grains" in the single crystal array.

Figs. 25 (b) to (f), 26 (a) to (e), and 27 (a) to (f) plot the magnitude of |α - β| against angle α for all MICAST and MICAST-G and the numerically simulated dendrite array respectively. There does not appear to be any growth rate dependence of |α - β| in MICAST or MICAST-G samples. Also, they both show similar |α - β|values. However, there appears to be larger scatter in |α - β| values of MICAST-G samples suggesting that natural convection affects the uniformity of side-branch morphology. The simulated dendrite array

(Fig. 27(a)) also shows large scatter in the |α - β|. As the morphology transitions from branched dendrite to more cell-like (Fg. 27(a) through 27(f)) the scatter in |α - β| value appears to increase. However, it could be an artifact introduced while drawing the lines corresponding to the mid-location of the branches.

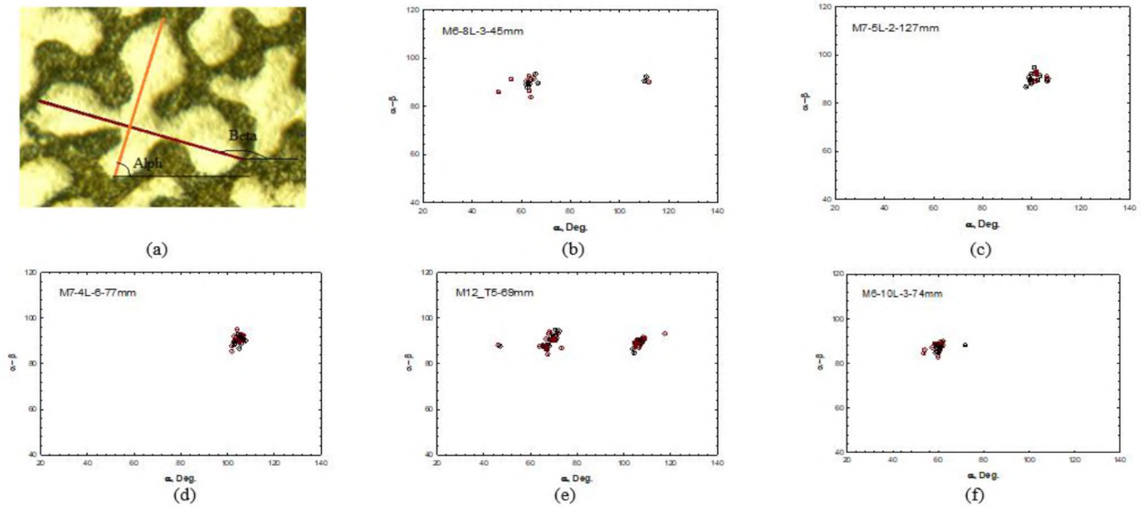

(a) (b) (c) (d) (e) (f)

Figure 25. Magnitude of |α - β| versus α graph of MICAST samples (a) Dendrite (b) M6-8L-3 (c) M7-5L2-1 (d) M7-4L-6 (e) M12-T5 (f) M6-10L-3

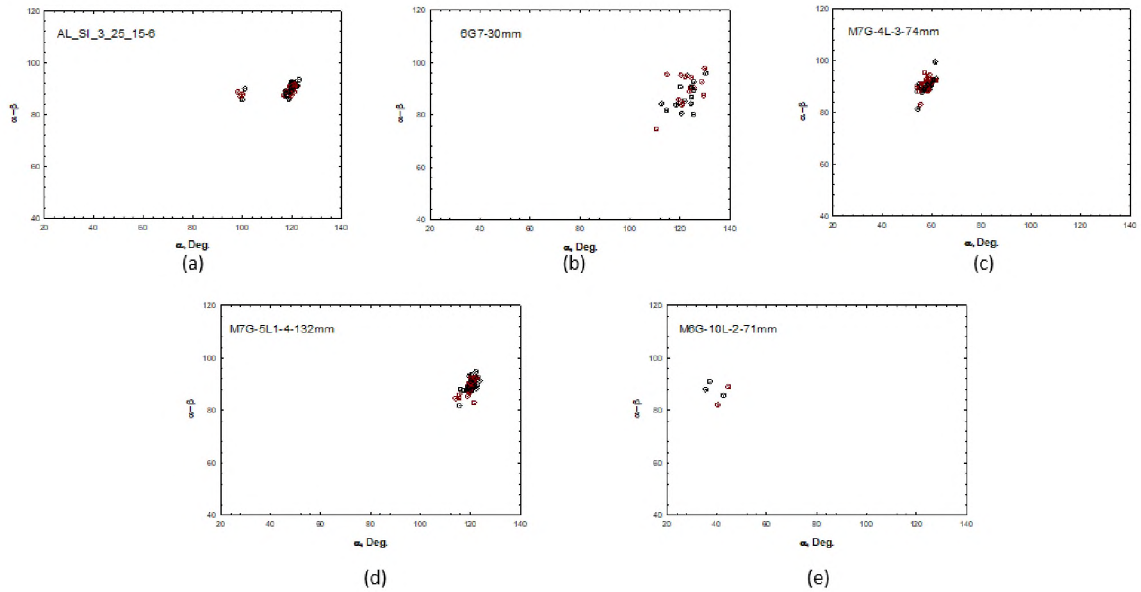

(a) (b) (c) (d) (e)

Figure 26.Magnitude of |α - β|versus α graph of MICAST-G samples (a) M6G-7T (b) M7G-5L1-4 (c) M7G-4L-3 (d) Al-Si-3-25-15-6 (e) M6G-10L-2

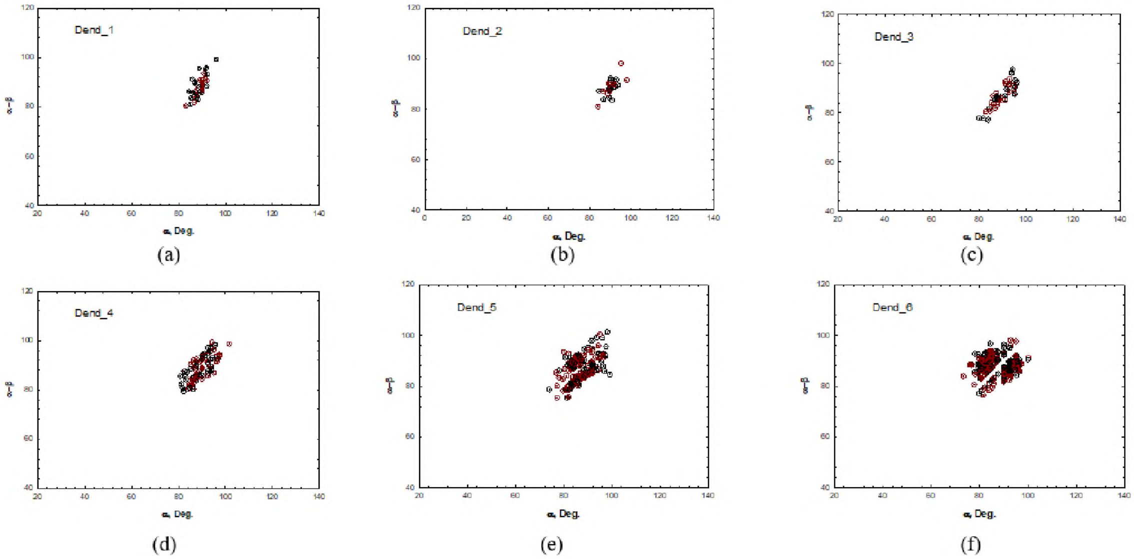

Figure 27.Magnitude of |α - β| versus α graph of simulated dendrites samples (a) Dend_1 (b) Dend_2 (c) Dend_3 (d) Dend_4 (e) Dend_5 (f) Dend_6

3.5 Misoriented (Spurious) Grains in MICAST and MICAST-G Samples

Fig. 28 (a) to (e) shows the transverse views of MICAST sample with the misoriented grains marked with a yellow circle. Similarly, Fig. 29 (a) to (e) are for the MICAST-G samples. Spurious grains are expected to form because of natural convection in the terrestrial grown samples when a side-arm gets detached from its tree (primary dendrite), grows into a new dendrite, and forms its own tree (primary dendrite). Therefore, the presence of spurious grains in the terrestrial samples (MICAST-G) is not surprising. But observation of such grains in Space Processed samples is quite surprising and unexpected. It indicates that the mushy-zone fluid may not have been quiescent during some of the samples processed in space[7,27-28].

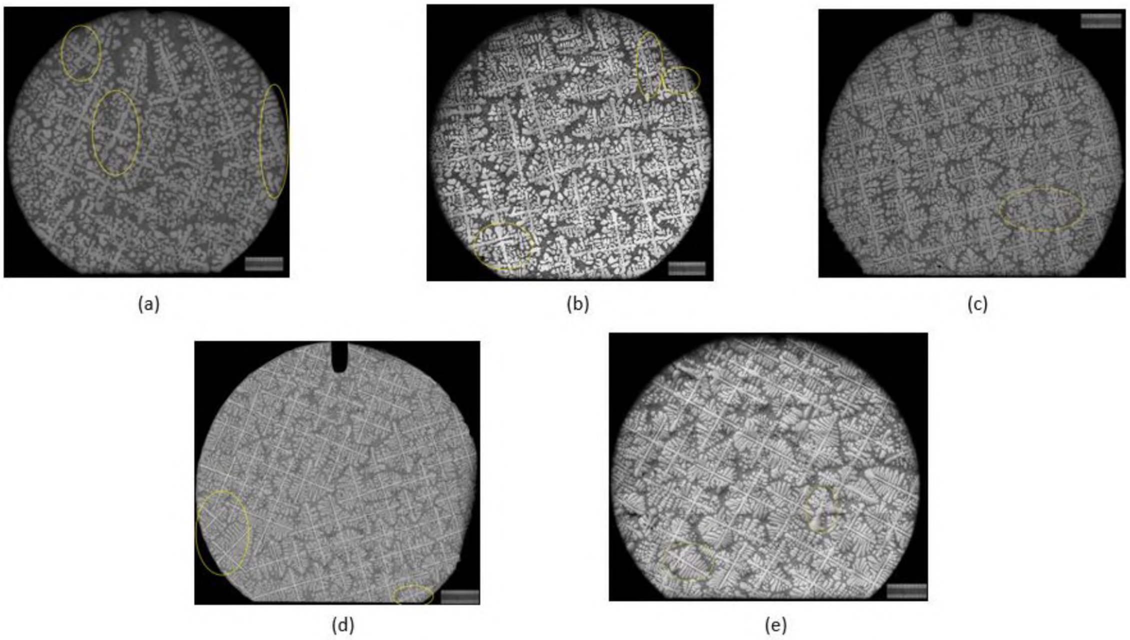

Figure 28.The misoriented grains in MICAST samples marked by yellow circles (a) M6-8L-3 (b) M7-5L2-1 (c) M7-4L-6 (d) M12-T5 (e) M6-10L-3

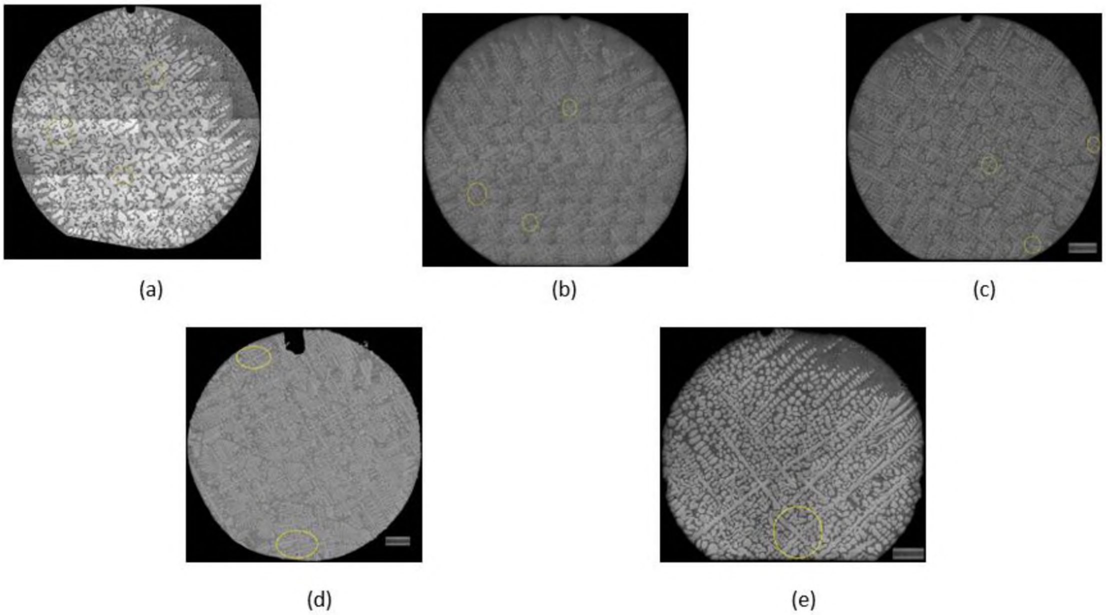

Figure 29. The misoriented grains in MICAST-G samples marked by yellow circles (a) M6G-7T (b) M7G-5L1-4 (c) M7G-4L-3 (d) Al-Si-3-25-15-6 (e) M6G-10L-2

3.6 Comparison of Micro-Gravity and Terrestrial Grown Samples

Table 5 lists the MICAST and MICAST-G samples which have been compared in this section. This comparison is an attempt to investigate if the presence of natural convection affects the morphology and distribution of primary dendrites. The growth speeds of the two sets of the samples are nearly identical to each other.

Table 5 MICAST and MICAST-G samples with their growth speed

Sample Number	MICAST	Velocity (μms^{-1})	MICAST-G	Velocity (μms^{-1})
1	M6-8L-3	5.6	M6G-7T	5
2	M7-5L2-1	10.8	M7G-5L1-4	10
3	M7-4L-6	21.2	M7G-4L-3	20
4	M12-T5	40	Al-Si-3-25-15-6	40
5	M6-10L-3	50	M6G-10L-2	50

Here, we examine the growth speed dependence of the morphology parameters examined in this study, secondary (side)-arm length ratio, L_1/L_2 (Fig. 30), the ratios of the opposite side-branches of the larger secondary-arm (d_1/d_2) (Fig. 31) and the ratio of the opposite side-branches of the shorter secondary arm (d_3/d_4) (Fig. 32). For each one of these two plots is presented, the first plot contains only the mean values plotted as a function of growth speed and the second plot contains the mean and plus-minus one standard deviation values also. The black symbols in these graphs are for the microgravity processed MICAST samples and the red symbols are for the terrestrially grown MICAST-G samples. Fig. 30 shows that the mean value of the secondary arm ratio (L_1/L_2) is independent of the growth speed for the MICAST-samples. The mean L_1/L_2 values are slightly higher than unity for both MICAST and MICAST-G samples. However, for the MICAST-G samples, it appears to increase with the growth speed. It is significantly larger than unity for the terrestrial sample grown at 50 μm/s. It is because of the “steepling” convection present in this sample which leads to a liquid-solid interface which is not flat, instead, some primary dendrites lead their neighbors which begins to lag further as the solidification proceeds. The lagging primary dendrites develop side-arms that are longer on the side where the melt is more solute rich. This makes one side-arm much larger than the one located orthogonal to it. Since the primary dendrites in the leading region of the mushy-zone have smaller primary-dendrite spacing than those located in the lagging region of the mushy-zone, it also results in a large scatter in the L_1/L_2 values as seen in the MICAST-G sample grown at 50 μms^{-1} (M6G-10L-2 sample). The L_1/L_2 value as high as 6 is seen in this sample which was significantly steepled.

Fig. 31 plots the ratio of the two opposite pairs of the side-branches which make the longer side-arm of the primary dendrite (d_1/d_2). Let us recall that the L_1/L_2 values are invariably larger than unity for all these samples, indicating that primary dendrite spacing along one <100> direction is larger than that along the corresponding normal <100> direction. One way to visualize this is that "one side of the cross is 30% to 100% longer than the other side"; mean d_1/d_2 varies from about 1.3 to 2 for the MICAST-G samples and from 1.3 to 1.6 for the MICAST samples. The side-branch anisotropy also appears to increase with increasing growth speed (Fig. 31(a)). Fig. 32 shows this side-branch anisotropy parameter as visualized from the opposite two branches of the cross (d_3/d_4). Here also the ratio is larger than unity for all the samples, whether they are space processed or terrestrially grown. For some dendrites, these ratios are as large as 6 (Fig. 31 and 32). Not only one dendrite arm is longer than the opposite arm, but the two arms also get split into highly unequal portions. The cross is not a true cross made up of equal side-arms, as has been long believed by the solidification community.

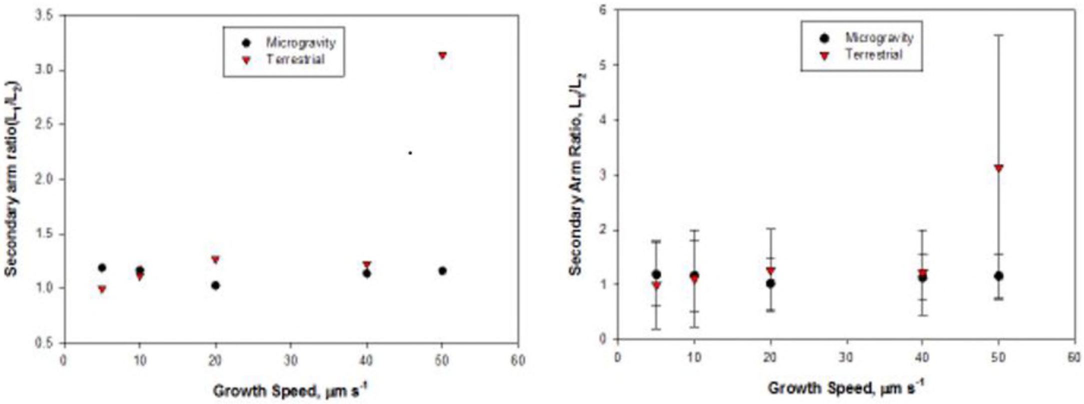

Figure 30. Growth speed dependence of the secondary (side)-arm length ratio, L_1/L_2 in MICAST nd MICAST-G samples.

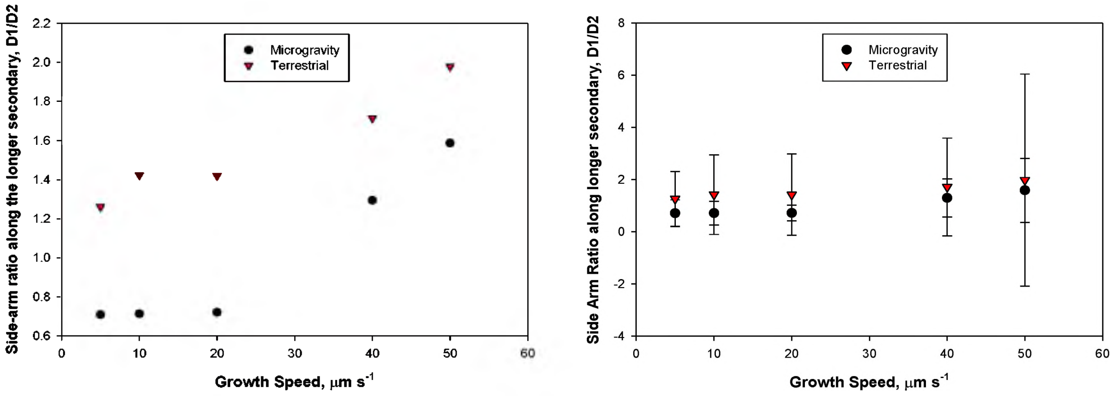

Figure 31. Growth speed dependence of the side-arm ratio along the longer secondary arm (d_1/d_2) in MICAST and MICAST-G samples.

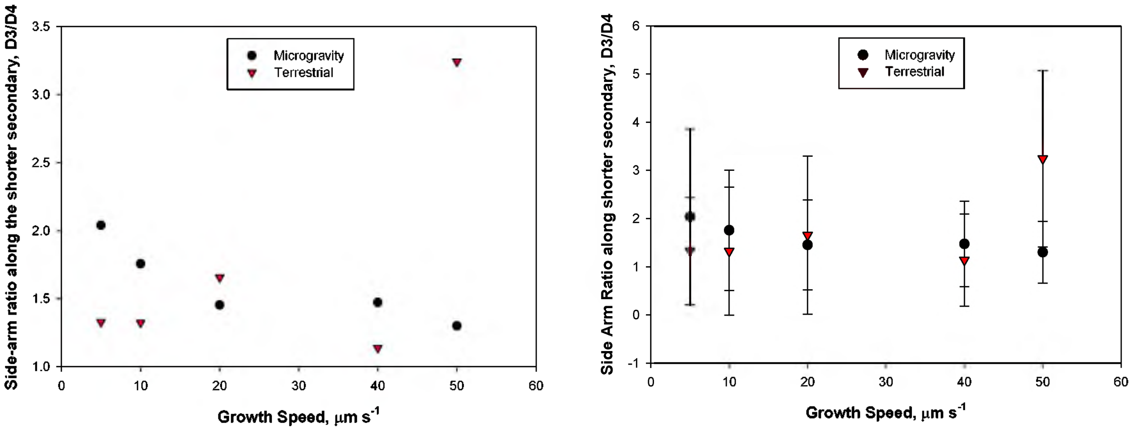

Figure 32. Growth speed dependence of the side-arm ratio along the shorter secondary arm (d_3/d_4) in MICAST and MICAST-G samples.

3.7 Pooled Analysis of the Morphology Parameters: MICAST, MICAST-G, and Simulated Dendrites Array

Here, we will attempt to compare the three sets of morphologies by pooling the data together. For example, the morphology parameters (L_1/L_2, d_1/d_2, d_3/d_4 and $\alpha-\beta$) of all five Space Station processed MICAST samples, irrespective of their growth speeds, are pooled together as a group to obtain their means and standard deviations. Tables 6, 7, and 8 respectively show the numerical values obtained from such an analysis for the three groups of morphologies examined in this study, the MICAST, MICAST-G, and the numerically simulated Dendrite Arrays for the L_1/L_2, d_1/d_2 and d_3/d_4, and $\alpha-\beta$ parameters. Fig. 33 compares these parameters for the MICAST, MICAST-G, and the numerically simulated Array. The MICAST samples' mean value is marked with black circles along with plus-minus one standard deviation represented by the straight line. The mean of the MICAST-G samples is represented by a red triangle and the standard deviation with the straight line. And the simulated dendrite array means are represented by a green square and standard deviation by straight-line respectively.

Fig. 33 shows that the side-arm ratio L_1/L_2 of the dendrites in the micro-gravity samples is greater than one, and it is also higher than that in the terrestrial samples. It is also interesting to note that the Coefficient of Variance of MICAST samples is significantly less than that of MICAST-G samples (Table-6). Unlike simulations where this value comes out to be unity the actual primary dendritic arrays growing undisturbed in a convection free environment invariably have one of their side-arms longer than its opposite counterpart. Theoretical analyses of primary dendrite arrays have all missed this basic point; they all come up with uniform trees having identical morphology distributed all through the single crystal garden.

The side-branch anisotropy parameter d_1/d_2 and d_2/d_3 also show this behavior, unlike the theoretical models these ratios are not unity but are larger than one. It is interesting to note that the MICAST samples show that their longer side-arm is split into two parts which are closer to unity (d_1/d_2) than the split of their shorter secondary arm (d_3/d_4). Again, it should be noted that the Coefficient of Variance of MICAST samples is less than that of MICAST-G samples for both (d_1/d_2) and (d_3/d_4) (Table-7). The mean value for the magnitude of |a-b| is close to 90° for both the micro-gravity and terrestrial samples. The coefficient of variance for |a-b| is significantly less in the MICAST samples as compared with the MICAST-G samples (Table-8).

Table 6 MICAST, MICAST-G, and Simulated dendrite samples combine Mean Value and Standard Deviation for side-branch anisotropy

	d1/d2				**d3/d4**			
	MEAN	Number	Standard Deviation	Coeff of Variation	MEAN	Number	Standard Deviation	Coeff of Variation
Space	1.1015	178	0.807	0.73264	1.526	178	1.04	0.68152
Terrestrial	1.5016	193	1.676	1.11614	1.224	193	0.915	0.74755
Simulated dendrites	0.8797	78	0.176	0.20007	1.059	78	0.172	0.16242

Table 7 MICAST, MICAST-G, and Simulated dendrite samples combine Mean Value and Standard Deviation for the secondary (side)-arm ratio

	L1/L2			
	MEAN	**Number**	**Standard Deviation**	**Coeff of Variation**
Space	1.4632	178	0.7615	0.52043
Terrestrial	1.2225	193	0.9151	0.74855
Simulated dendrites	0.9981	78	0.154	0.15429

Table 8 MICAST, MICAST-G and Simulated Dendrite Samples Combine Mean Value and Standard Deviation of Magnitude ($\alpha-\beta$)

	($\alpha-\beta$)			
	MEAN	**Number**	**Standard Deviation**	**Coef. Of Variation**
Space	89.46	178	2.26	0.02526
Terrestrial	89.513	193	3.2	0.03575
Simulated dendrites	87.81	78	4.3638	0.049

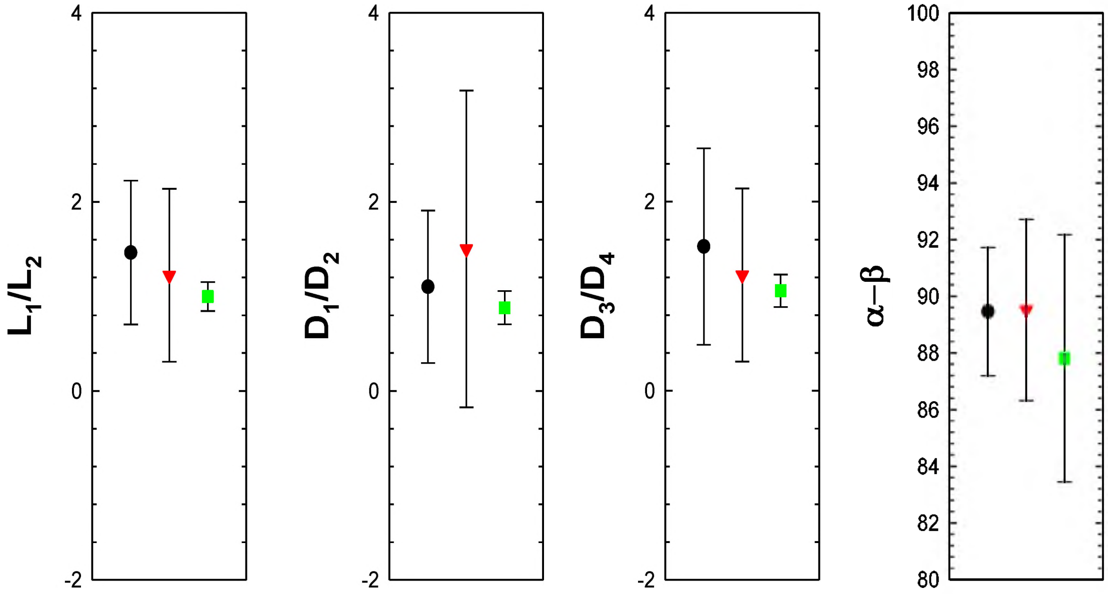

Figure 33.Comparison of morphology parameters, L_1/L_2, d_1/d_2, d_3/d_4, and a-b of the three groups of dendrites examined in this study. MICAST samples (Black circles), Terrestrial MICAST-G samples (red triangles), and numerically Simulated branched dendrite array (green squares).

3.7.1 T-Test Analysis of MICAST, MICAST-G, Samples and Simulated Dendrite Arrays

In order to make statistically valid observations regarding these morphology parameters of the three sets of morphologies examined here the "t-test" was utilized. The t-test is a hypothesis test that permits you to compare the means of two groups of data. It evaluates whether the means of two groups are statistically different from each other. The T-Test is done using sigma plot application by supplying the group mean, the standard deviation, and the number of data points in the two groups, shown in tables 6, 7, and 8. The test is run in a pair of MICAST vs Terrestrial (MICAST-G) and MICAST vs simulated dendrites for all four morphology parameters.

The test results are shown in Table 9 in the form of the t-value and p-value. The t-value is simply the calculated difference between the mean value of two groups in units of standard error. The greater the magnitude of the t-value, the greater will be the difference and the closer t-value is to 0, the more probability that there is no considerable difference. Whereas the p-value is the calculated probability of obtaining the remarked or radical result of t-value.

Table 9 MICAST Vs Terrestrial, and MICAST Vs Simulated Dendrite Samples T-test

	L_1/L_2		**d_1/d_2**		**d_3/d_4**		**Mag ($\alpha-\beta$)**	
	t	**p**	**t**	**p**	**t**	**p**	**t**	**p**
MICAST vs. Terrestrial	2.741	0.862	-2.891	0.893	2.975	0.907	-0.183	0.072
MICAST vs. Simulated Dendrites	5.341	1	2.4	0.773	3.938	0.989	3.978	0.99

Base on this analysis following conclusions can be made:

3.7.1.1 MICAST Samples Vs. Numerically Simulated Dendrites

- The mean secondary Branch ratio of micro-gravity processed MICAST samples is larger than the simulated dendrites sample.
- The mean value of the side-arm ratio along the longer secondary of the micro-gravity processed MICAST samples is larger than simulated dendrites samples.
- The mean value of the side-arm ratio along the shorter secondary of the micro-gravity processed MICAST samples is larger than the simulated dendrites sample.

- The extent of orthogonality (α - β) of the secondary branches is larger in the micro-gravity processed MICAST than in simulated dendrites.

3.7.1.2 MICAST Samples Vs. Terrestrial Samples.

- The mean secondary Branch ratio of micro-gravity processed MICAST samples is larger than the terrestrial samples.
- The mean value of the side-arm ratio along the longer secondary of the micro-gravity processed MICAST samples is smaller than terrestrial samples.
- The mean value of the side-arm ratio along the shorter secondary of the micro-gravity processed MICAST samples is larger than terrestrial samples.
- The extent of orthogonality (α−β) of the secondary branches is similar in the micro-gravity processed MICAST and terrestrial samples.

3.8 Fast Fourier Transform (FFT) of Typical MICAST, MICAST-G, and Simulated Dendrite Arrays

Fast Fourier Transform represents an image in the frequency domain by decomposing an image into its real and imaginary components. The input image for transformation is represented as the frequency domain and the output is represented as spatial domain. It may provide another mechanism to quantitatively compare the pattern formation and the disorder hidden in the images so far as the repeatability of dendrites in a dendritic array is concerned[29-30]. In other words, how well are the primary dendrite trees arranged in the single crystal garden of the solidifying binary alloy? The preliminary analysis reported here indicates that this technique has a strong potential and should be further explored.

Here we transform typical transverse images of MICAST, MICAST-G, and simulated array samples into their Fourier transforms using ImageJ software. Fig. 34 (a), (b), and (c) shows the images of MICAST, MICAST-G, and the simulated dendrite arrays. Fig. 34 (e), (f), and (g) show the Fourier transform of the corresponding images. The red lines are drawn in the microstructural images (Fig 34(a) through (d)) to indicate the directions along which the dendritic pattern appears to repeat itself as we move radially outward from the image centers.

FFT of the simulated array Fig. 34(f) shows a pattern that can represent a hexagonal distribution of lattice points with radial noise superimposed on the array points. However, such a FFT can also result from a square lattice having superimposed random noise. In any case, this pattern has identifiable points along with zero, 90, and 120° directions. As opposed to this the MICAST sample (Fig. 34(d)) shows "streaking" along with zero and 90°. The streaks are symmetrical on their two radially opposite directions.

This is likely to result from the fact that the dendrites in MICAST samples have much longer side arms which have their own side-arms, as compared to the simulation where the side-arms are not well-branched. The MICAST-G sample FFT (Fig, 34(d)) shows additional streaking along 120°. For this sample streaking along 0 and 90° are radially symmetrical indicating the formation of dendrites with side-branch in the two directions. But the streak along 120° is not radially symmetric. The reason for this behavior is presently not understood. However, from this very preliminary analysis, it is apparent that FFT of the transverse microstructures has a strong potential to be used as a quantitative analysis tool to measure the nature of the pattern formation in dendritic arrays, and the disorder present therein.

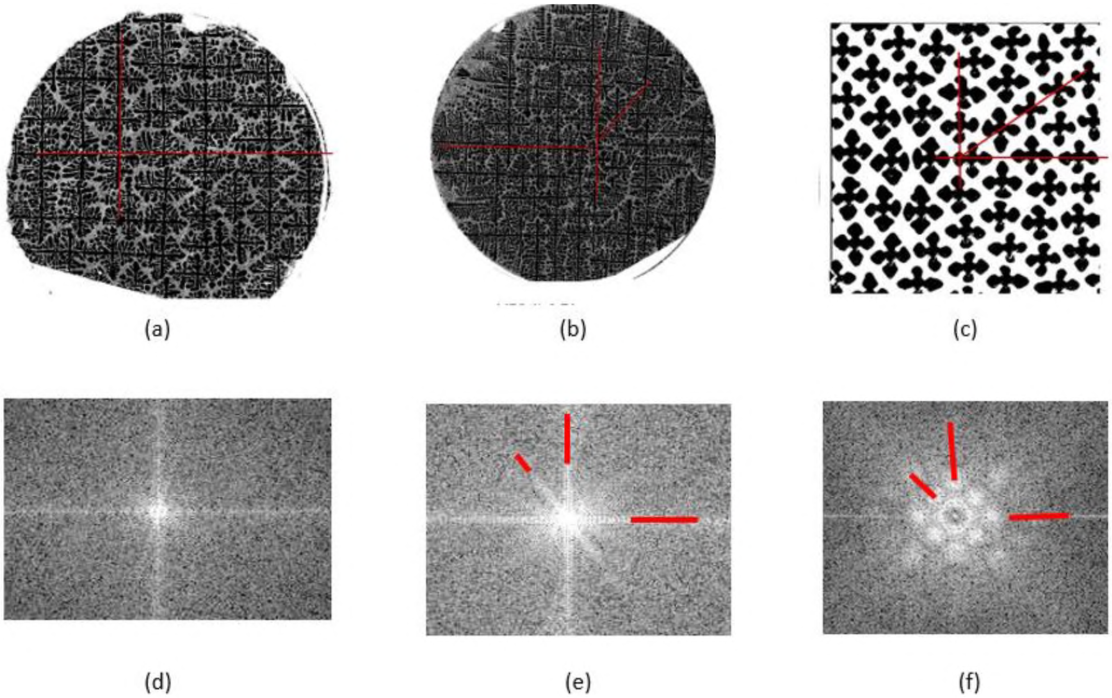

(a) (b) (c)

(d) (e) (f)

Figure 34. Pattern formation in simulated dendrites and MICAST-G samples (a) Image of MICAST sample M7-4L-6-77mm (b) Image of MICAST_G sample M7G-4L-3-74mm (c) Image of Simulated Dendrites sample (d) Fourier transform the image of MICAST sample M7-4L-6-77mm (e) Fourier transform the image of MICAST_G sample M7G-4L-3-74mm (f) Fourier transform the image of Simulated Dendrites sample

CHAPTER IV

SUMMARY AND CONCLUSION

The purpose of this research is to examine the ordering in the Primary Dendrite Pattern formation during directional solidification of binary face-centered-cubic (fcc) metallic alloys along [100] direction, and explore what kind of disorder is introduced in the dendritic array by natural convection. Al-7%Si alloy samples directionally solidified terrestrially in our lab at CSU (in the presence of natural convection), and those directionally solidified on the International Space Station (in the absence of convection) have been analyzed and the dendrite patterns in these samples have been compared with each other. In addition Al-3%, Cu dendritic patterns obtained by numerical simulation (assuming diffusive mass transport) carried-out by Japanese Researchers [25] have been analyzed and compared with those in the Al-7%Si samples. Transverse microstructures of five samples, grown at speeds varying from 5 to 50 μms^{-1}, from the Space Station Processed group (MICAST) and terrestrially solidified group (MICAST-G) have been analyzed for the morphology and distribution of primary dendrites on the sample cross-section.

All dendrites in each sample were examined to measure the lengths of their two orthogonal secondary side-arms (L_1 and L_2), split of the two side-arms into their two halves (d_1 and d_2 for L_1, and d_3 and d_4 for L_2), and the angles of the two side arms with respect to horizontal (α for L_1 and β for L_2). Computer programs were developed to augment the image processing tools available from ImageJ and MATLAB for this purpose. It is generally believed that in an fcc alloy the primary dendrites growing along [100] direction in a quiescent environment (absence of convective flows) will have orthogonal side-arms ($|\alpha-\beta|=90^o$) and, the side-arms would be of equal lengths ($L_1/L_2=1$) and would be split equally into their side-branches ($d_1/d_2=1$ and $d_3/d_4=1$). It is also believed that such a dendrite morphology is uniformly distributed across the entire sample cross-section for a single crystal sample.

Fast Fourier Transformation of the transverse images selected from the three groups, MICAST, MICAST-G, and numerically simulated has been explored to examine if such an analysis can be used as another measure to evaluate the quality and scatter in the dendrite-patterns formed during directional solidification.

The following presents a summary of the important observations made by this study.

1. The number of dendrites seen on the cross-section increases and the randomness in the orientation of dendrites appears to decrease as the growth speed increases for both the MICAST and MICAST-G group of samples.
2. The side-arms of primary dendrites are not exactly orthogonal in either the MICAST or MICAST-G samples even though they are growing along [100] direction, suggesting that there may be an inherent scatter in the orthogonality of side-arms of neighboring primary dendrites which is not accounted for in the present theoretical models. No growth rate dependence of $|\alpha - \beta|$ was seen in the MICAST or MICAST-G samples, even though the side-arms become more branched as the growth rate increases.

3. The mean L_1/L_2 values are slightly higher than unity for both MICAST and MICAST-G samples, unlike the simulated dendrite array where L_1/L_2 is unity. The side-arm anisotropy (L_1/L_2) is independent of the growth speed for the low gravity processed MICAST-samples. However, in the terrestrial processed samples, it appears to increase with the growth speed. Numerical simulations or dendrite theories need to account for this observation that real dendrites look more like trees with interpenetrating side branches growing into the nearby space available, and are not restricted to having equal side-arms.
4. The side-arms are split into nearly equal two halves in the simulated dendrite array (d_1/d_2 and d_3/d_4 are close to unity). However, the actual primary dendrites in either the MICAST or the MICAST-G samples show these ratios to be as large as 6. It is also interesting that the MICAST samples grown in low-gravity appear to have larger d_1/d_2 or d_3/d_4 values as compared with the MICAST-G samples. The numerical simulations or dendrite theoretical models do not yet account for this behavior.
5. When the morphology parameters are pooled together for all the MICAST samples (irrespective of their growth speed) and also for the MICAST-G samples to compare the two groups, it is observed that,
    a) The side-arm ratio L_1/L_2 of the dendrites in the micro-gravity samples is greater than one, and it is also greater than that in the terrestrial samples. The primary dendrites growing in the convection-free environment invariably have one of their side-arms longer than its opposite counter-part, unlike simulations where this value comes out to be unity.

b) The side-branch anisotropy parameter d_1/d_2 and d_3/d_4 in MICAST and MICAST-G samples are also larger than unity, unlike the theoretical models where these ratios are predicted to be unity.

c) Mean $|\alpha - \beta|$ values of both MICAST and MICAST-G samples are close to 90^o indicating overall orthogonality of secondary arms, but there is large scatter around this mean.

d) Standard of Variance for all the four parameters, L_1/L_2, d_1/d_2, d_3/d_4, and $|\alpha - \beta|$ is less in the micro-g processed MICAST samples than in terrestrial processed MICAST-G samples indicating that natural convection does increase the extent of disorder (noise) in the dendrite morphology and their distribution.

6. The earth-grown samples M6G-7T and M6G-10L-2 with a growth speed of 5 and 50 μms^{-1} show severe "steepling" convection, which results in extensive radial macro-segregation and dendrites being non-uniformly distributed. However, the Space-Station processed sample with a growth speed of 5 μms^{-1} also shows evidence of such convection. The presence of misoriented (spurious) grain in this MICAST sample indicates that at least this sample was subjected to some sort of fluid flow even though it was grown under the quiescent conditions of Space. It may be attributed to Marangoni convection caused by a liquid column (detached from the crucible walls) existing under an imposed thermal gradient, as has been observed by Supriya Upadhyay[7].

7. Fast Fourier Transforms of typical transverse images of dendrite array in MICAST, MICAST-G, and Numerically Simulated dendrite samples show significant differences. This should further be explored as a technique to measure the degree of

noise present in the morphology and distribution of primary dendrites in a quantitative manner. Image analysis using entropy as a parameter in the micro-structure and FFT should also be explore.

REFERENCES

1. Stefanescu, D.M., "*Science and Engineering of Casting Solidification*", Springer, vol. 2, pp. 67-68, (2009)
2. Jonathan, A.D. Michel, R., "*Solidification,* Engineering science, 2nd Edition", pp 5-12.
3. Al-Rawahi N, Tryggvason G., *"Numerical simulation of dendritic solidification with convection: Three-dimensional flow"*. Journal of Computational Physics. 2004;194 (2):677-696. doi: http://dx.doi.org/10.1016/j.jcp.2003.09.020.
4. Burden M.H. and Hunt J.D., "Cellular and dendritic growth. I", *Journal of Crystal Growth.*, 22(1974), 99-108.
5. Lu SZ and Hunt JD, "A numerical analysis of dendrite and cellular array growth: the spacing adjustment mechanism", *J. Cryst. Growth (1992)* **123** 17-34.
6. M.D. Dupouy, D. Camel, and J.J. Favier, "*Natural convective effects in directional dendritic solidification of binary metallic alloys: dendritic array morphology".* *Journal of Crystal Growth.*, 1993, vol. 126, pp. 480-88.
7. Supriya, R.U., "*Spurious Grain Formation During Directional Solidification in Microgravity"*. MS Thesis. Cleveland State University; 2018.
8. Ghods, M. Johnson, L. Lauer, M. Grugel, R.N. Tewari, S.N. Poirier, DR. "*Radial macrosegregation and dendrite clustering in directionally solidified Al–7Si and Al–19Cu alloys"*. Journal of Crystal Growth. 2016; 441:107-116. doi: http://dx.doi.org/10.1016/j.jcrysgro.2016.02.014
9. Angart, S. Lauer, M. Tewari, S.N. Grugel, R.N. Poirier, D.R. "*Comparison of directionally solidified samples solidified terrestrially and aboard the international space station."* Proceedings of 61st Annual Technical Conference of the Investment Casting Institute, Covington, KY, Oct. 5 – 8, Paper 6, 2014.

10. Tewari, S.N. Tewari, R. Magadi, G.: "*Mushy Zone Rayleigh Number to Describe Macrosegregation and Channel Formation in Directionally Solidified Metallic Alloys", Metall.* Materials Trans. 2004 (35A) 2927-2934.
11. Rappaz, M. Gandlin, Ch.-A. Desbiolles, J.L. Thevoz, Ph. "*Prediction of grain structures in various solidification processes"*, Metall. Materials. Trans. 27A (1996) 695-705.
12. Gandin, Ch-A. Rappaz, M. "*A coupled finite element-cellular automaton model for the prediction of dendritic grain structures in solidification processes*." Acta Metall. Materialia 42.7 (1994): 2233-2246.
13. Gandlin, Ch.-A. Desbiolles, J.L. Rappaz, M. Thevoz. Ph. "*A Three-Dimensional Cellular Automaton–Finite Element Model for the Prediction of Solidification Grain Structures"*, Metall. Materials. Trans. 30A (1999) 3153-3165.
14. Grugel, R. Brush, L. Anilkumar, A. *"Disruption of an Aligned Dendritic Network by Bubbles during Re-melting in a Microgravity Environment"*, 50th AIAA Aerospace Sciences Meeting, 9 - 12 Jan 2012, 26th Symposium on Gravity - Related Phenomena in Space Exploration.
15. Poirier, D. Zhao P.and Heinrich, J. "*Dendritic Solidification of Binary Alloys with Free and Forced Convection",* Int. J. Numer. Meth. Fluids, vol. 49, pp. 233-266, 2005
16. Ghods, M. Tewari, S.N. Lauer, M. Poirier, D.R. Grugel R.N. "*Processing parameter dependence of primary dendrite spacing and trunk diameter in Al-7 wt% Si alloy directionally solidified aboard the International Space Station",* American Society for Gravitation and Space Research Annual Meeting, Cleveland, OH, Oct 25-29, 2016. (https://ntrs.nasa.gov/archive/nasa/casi.ntrs.nasa.gov/20160013345.pdf)

17. M.D. Dupov and D. Camel, Effects of gravity on columner dendritic growth of metallic alloys: flow pattern and mass transfer, J. Crystal Growth. 183 (1998) 469-489.
18. H.N. Thi, Y. Dabo, B.Drevet, M.D. Dupouy, D. Camel, B. Billia, J.D. Hunt and A. Chilton. Directional solidification of Al-1.5 wt% Ni alloys under diffusion transport in space fluid-flow localization on earth. J. Crystal Growth 281 (2005) 654-668.
19. B. Drevet, H.N. Thi, D. Camel, B. Billia and M.D. Dupouy. Solidification of aluminum-lithium alloys near the cell/dendrite transition-influence of solutal convection. J. Crystal Growth. 218 (2000) 419-433.
20. Upadhyay, S.R. Tewari, S.N. Ghodes, M. Grugel, R.N. Poirier, D.R. and Lauer, M. *"Primary Dendrite Trunk Diameter in Al-7wt% Alloy Directionally Solidified Aboard the International Space Station", 2019 IOP Conf. Ser.: Mater. Sci. Eng. 529 012022.*
21. Shan Liu, Shu-Zu Lu, Hellawell A.: "*Dendritic array growth in the systems NH4Cl–H2O and [CH2 CN]2–H2O: "The detachment of dendrite side arms induced by deceleration*, J. Crystal Growth 234 (2002) 740–750.
22. Mathiesen, R.H. Arnmerg, L. Bleuet, P.and Somogyi A. *"Crystal Fragmentation and Columnar-to-Equiaxed Transitions in Al-Cu Studied by Synchrotron X-Ray Video Microscopy"*, Metall. Materials. Trans. 37A (2006) 2515-2524.
23. Ruvalcaba, D. Mathiesen, R.H. Eskin, D.G. Arnberg, L. and Katgerman, L. "*In situ observations of dendritic fragmentation due to local solute-enrichment during directional solidification of an aluminum alloy"*, Acta Materialia 55 (2007) 4287–4292.

24. Kermanpur, A., et al.: "*Thermal and grain-structure simulation in a land-based turbine blade directionally solidified with the liquid metal cooling process"*. Metall. Materials Trans. 31 (2000) 1293-1304.
25. Tomohiro, T.A. Shinji, S.B. Munekazu, O.C. Yasushi, S.D.Takashi, S.E. Takayuki, and A.E. "*Primary arm array during directional solidification of a single-crystal binary alloy: Large-scale phase-field study*", *Acta Materialia* 118 (2016) 230-243.
26. S. Steinbach, "*First results of the MICAST Experiments in MSL onboard the ISS*", Institute of Material Physics in Space, German Aerospace Center (DRR), Cologne, (2012).
27. Avenson, J.W., G. Goddard C.J.L. Nugyen-thi, H. Mangelinck-noel, N. Tandjaoui, A. Davenport, J.R. Warnken, N. Gioacchino, F.D. Lafford, T.A. D'souza, N. Billia, B. and Stone, H.J. *"On the deformation of dendrites during directional solidification of a nickel-based superalloy", Metallurgical and Materials Transactions A*, (2019) pp, 5234-5240
28. Nabavizadeh, S.A. Eshraghi, M. Felicelli, S.D. Tewari, S.N. and Grugel, R.N. *"Effect of Bubble-induced Marangoni Convection on Dendritic Solidification International"*, Journal of Multiphase Flow 116 (2019) 137-152.
29. Jain, A. "*Fundamentals of Digital Image Processing"*, Prentice-Hall, 1989, pp 15 – 20
30. Marion, A. "*An Introduction to Image Processing"*, Chapman and Hall, 1991, Chap. 9.

APPENDIX

Orientation Measurements (Matlab Code)

Arm length

```
clc;
clear all;
ExcelFile= uigetfile;
raw=xlsread(ExcelFile);  %% the numerical values of the excel file will sit in a matrix
called raw
[r, c]=size(raw);  % r is number of rows and c is number of columns in data excel file
scale=370;  % number of pixels per mm in original image

%%% the for loop scans pairs of the line in the "raw" matrix
for n=1:r/2
% this if takes care of the regular drawn lines. The sixth element of
% each row is the angle and the decision about the use of BX and BY as a known point
% on the drawn line is based on this angle value


% 1st line 2nd and 4th quadrant
    if ((raw(2*n-1,6)<0) && (raw(2*n-1,6)> -90)) || ((raw(2*n-1,6)> 90) && (raw(2*n-
1,6)< 180))
    X1=raw(2*n-1,2);
    Y1=raw(2*n-1,3);
    X3=raw(2*n-1,2)+raw(2*n-1,4);
    Y3=raw(2*n-1,3)+raw(2*n-1,5);
    X2=raw(2*n,2);
    Y2=raw(2*n,3)+raw(2*n,5);
    X4=raw(2*n,2)+raw(2*n,4);
    Y4=raw(2*n,3);
    m1=-tand(raw(2*n-1,6));
    m2=-tand(raw(2*n,6));
    X=(m1*X1-Y1+Y2-m2*X2)/(m1-m2);
    Y=m1*(X-X1)+Y1;


  % 1st line 1nd and 3th quadrant
else if ((raw(2*n-1,6)<90) && (raw(2*n-1,6)> 0)) || ((raw(2*n-1,6)> -180) && (raw(2*n-
1,6)< -90))
    X1=raw(2*n-1,2)+raw(2*n-1,4);
    Y1=raw(2*n-1,3);
    X3=raw(2*n-1,2);
    Y3=raw(2*n-1,3)+raw(2*n-1,5);
```

```
        X2=raw(2*n,2);
        Y2=raw(2*n,3);
        X4=raw(2*n,2)+raw(2*n,4);
        Y4=raw(2*n,3)+raw(2*n,5);
        m1=-tand(raw(2*n-1,6));
        m2=-tand(raw(2*n,6));
        X=(m1*X1-Y1+Y2-m2*X2)/(m1-m2);
        Y=m1*(X-X1)+Y1;
         end
    end

    %%%%%% special cases start here %%%%%%%%



    % this if makes decision about the use of BX and BY in case the first line in a pair is
vertical
    % and the second one is either in first or in third quadrant
if ((raw(2*n-1,6)== 90) || (raw(2*n-1,6)== -90)) && (((raw(2*n,6)<90) &&
(raw(2*n,6)> 0)) || ((raw(2*n,6)> -180) && (raw(2*n,6)< -90)))
    X1=raw(2*n-1,2);
    Y1=raw(2*n-1,3);
    X3=raw(2*n-1,2);
    Y3=raw(2*n-1,3)+raw(2*n-1,5);
    X2=raw(2*n,2);
    Y2=raw(2*n,3)+raw(2*n,5);
    X4=raw(2*n,2)+raw(2*n,4);
    Y4=raw(2*n,3);
    m2=-tand(raw(2*n,6));
    X=raw(2*n-1,2);
    Y=m2*(X-X2)+Y2;
    end

    % this if makes decision about the use of BX and BY in case the first line in a pair is
vertical
    % and the second one is either in forth or in second quadrant
    if ((raw(2*n-1,6)== 90) || (raw(2*n-1,6)== -90)) && (((raw(2*n,6)<0) &&
(raw(2*n,6)> -90)) || ((raw(2*n,6)> 90) && (raw(2*n,6)< 180)))
    X1=raw(2*n-1,2);
    Y1=raw(2*n-1,3);
    X3=raw(2*n-1,2);
    Y3=raw(2*n-1,3)+raw(2*n-1,5);
    X2=raw(2*n,2);
    Y2=raw(2*n,3);
    X4=raw(2*n,2)+raw(2*n,4);
    Y4=raw(2*n,3)+raw(2*n,5);
```

```
   m2=-tand(raw(2*n,6));
   X=raw(2*n-1,2);
   Y=m2*(X-X2)+Y2;
   end
    % this if makes decision about the use of BX and BY in case the first
   % line in a pair is horizontal
   % and the second one is either in first or in third quadrant
   if ((raw(2*n-1,6)== 0) || (raw(2*n-1,6)== 180)) && (((raw(2*n,6)<90) &&
(raw(2*n,6)> 0)) || ((raw(2*n,6)> -180) && (raw(2*n,6)< -90)))

   X1=raw(2*n-1,2);
   Y1=raw(2*n-1,3);
   X3=raw(2*n-1,2)+raw(2*n-1,4);
   Y3=raw(2*n-1,3);
   X2=raw(2*n,2);
   Y2=raw(2*n,3)+raw(2*n,5);
   X4=raw(2*n,2)+raw(2*n,4);
   Y4=raw(2*n,3);
   m2=-tand(raw(2*n,6));
   Y=raw(2*n-1,3);
   X=(Y-Y2)/m2+X2;
   end

   % this if makes decision about the use of BX and BY in case the first
   % line in a pair is horizontal
   % and the second one is either in forth or in second quadrant
   if ((raw(2*n-1,6)== 0) || (raw(2*n-1,6)== 180)) && (((raw(2*n,6)<0) &&
(raw(2*n,6)> -90)) || ((raw(2*n,6)> 90) && (raw(2*n,6)< 180)))

   X1=raw(2*n-1,2);
   Y1=raw(2*n-1,3);
   X3=raw(2*n-1,2)+raw(2*n-1,4);
   Y3=raw(2*n-1,3);
   X2=raw(2*n,2);
   Y2=raw(2*n,3);
   X4=raw(2*n,2)+raw(2*n,4);
   Y4=raw(2*n,3)+raw(2*n,5);
   m2=-tand(raw(2*n,6));
   Y=raw(2*n-1,3);
   X=(Y-Y2)/m2+X2;
   end
  % this if makes decision about the use of BX and BY in case the first
   % line in a pair is horizontal
   % and the second one is vertical
   if ((raw(2*n-1,6)== 0) || (raw(2*n-1,6)== 180)) && ((raw(2*n,6)== 90) ||
(raw(2*n,6)== -90))
```

```
  X1=raw(2*n-1,2);
  Y1=raw(2*n-1,3);
  X3=raw(2*n-1,2)+raw(2*n-1,4);
  Y3=raw(2*n-1,3);
  X2=raw(2*n,2);
  Y2=raw(2*n,3);
  X4=raw(2*n,2);
  Y4=raw(2*n,3)+raw(2*n,5);
  X=raw(2*n,2);
  Y=raw(2*n-1,3);
  end

  % this if makes decision about the use of BX and BY in case the first
  % line in a pair is vertical
  % and the second one is horizontal
  if ((raw(2*n-1,6)== 90) || (raw(2*n-1,6)== -90)) && ((raw(2*n,6)== 0) ||
(raw(2*n,6)== 180))

  X1=raw(2*n-1,2);
  Y1=raw(2*n-1,3);
  X3=raw(2*n-1,2);
  Y3=raw(2*n-1,3)+raw(2*n-1,5);
  X2=raw(2*n,2);
  Y2=raw(2*n,3);
  X4=raw(2*n,2)+raw(2*n,4);
  Y4=raw(2*n,3);
  X=raw(2*n-1,2);
  Y=raw(2*n,3);
  end

  % distance between two points
  d1 = sqrt((X3-X)^2+(Y3-Y)^2);
  d3 = sqrt((X2-X)^2+(Y2-Y)^2);

  % putting the calculated X and Y corresponding to center of dendrite
  % and each dendrites arm length in proper place in result matrix
  result(n,1)=n;
  result(n,2)=X;
  result(n,3)=Y;
  result(n,4)=X3;
  result(n,5)=Y3;
  result(n,6)=X1;
  result(n,7)=Y1;
  result(n,8)=d1;
  result(n,9)=raw(2*n-1,7)-d1;
```

```
    result(n,10)=raw(2*n-1,6);
    result(n,11)=d1/(raw(2*n-1,7)-d1);
    result(n,12)=X2;
    result(n,13)=Y2;
    result(n,14)=X4;
    result(n,15)=Y4;
    result(n,16)=d3;
    result(n,17)=raw(2*n,7)-d3;
    result(n,18)=raw(2*n,6);
    result(n,19)=d3/(raw(2*n,7)-d3);
    result(n,20)=raw(2*n-1,7)/raw(2*n,7);

end

% creating output excel file 1
filename = 'Dendrite_arm_length.xlsx';
A = {'ID','X','Y','X1','Y1','X2','Y2','d11','d12','Alph','d111/d12','X3','Y3','X4','Y4','d21','d22','Beta','d21/dH22','L1/L2'};
xlswrite(filename,A,1)
xlRange = 'E1';
xlswrite(filename,result,1,'A2')
```

Angle Sorting

```
clc; clear all
ExcelFile= uigetfile;
raw=xlsread(ExcelFile);  %% the numerical values of the excel file will sit in a matrix called raw
[r c]=size(raw);                        % r is number of rows and c is number of columns in data excel file
OUT=sortrows(raw,6);    %raw sorted based on row (6) i.e.angles.
angles=OUT(:,6);
binsize=2;                              %using bins which are 2 deg wide
nbins=round ((max(angles)-min(angles))/binsize);
[n,angle]=hist(angles,nbins);
plot(angle,n, '.k');
xlabel('Angle, deg');
ylabel('number');
    %Now open APPS TAB, select angle as X data and n as Y data
    %change the model type to Gaussian, input a suitable number of peaks
    %a is height, b is mean, and c/1.414 is the standard deviation.
    %You can also find the peak locations using the following program
[value,X]=findpeaks(n,angle);
GMModel=fitgmdist(angle',5) %find five gaussian peaks
```

```
%sorted=sort(angles);
%plot(sorted);
%[PKS,LOCS]=findpeaks(sorted,INDEX)
%N=10;
%for i=1:r-N
% x=sorted(i:i+N);
% y=[i:i+N]';
% coefficients=polyfit (x,y,1);
% slope(i)=coefficients (1);
%end
%plot (sorted',slope,'-r', xlabel('Angle, deg.'),ylabel('slope(num/deg)'));
%[PKS,LOCS] = findpeaks(slope,mod(:,1));
%figure (1)
%[N,Center] = hist(sorted);
%plot(Center, N);

%[f,xi] = ksdensity (sorted,Center);
%dN = mode (diff(Center));
%plot (Center,N/dN,'.- k',Center,N/dN,'.- b',xi,f*length(sorted),'.- r');
%legend ('Default','ksdensity');

%FX = gradient (sorted);
%plot FX;
```

Draw lines

```
clc;
ExcelFile= uigetfile;
raw=xlsread(ExcelFile);  %% the numerical values of the excel file will sit in a matrix called raw
[r, c]=size(raw);   % r is number of rows and c is number of columns in data excel file

for n=1:r
if (114<raw(n,10)) && (raw(n,10)<124) % this number depends upon the range of peek we got form angle slorting graph
    plot ([raw(n,4) raw(n,6)],[-raw(n,5) -raw(n,7)], '- b');
    hold on;
    plot ([raw(n,12) raw(n,14)],[-raw(n,13) -raw(n,15)], '- b');
    hold on;
    end
end
%% if number if peaks are more, more loop need to form

hold off;
```